ESAIM: M2AN 58 (2024) 1–22
https://doi.org/10.1051/m2an/2023097

ESAIM: Mathematical Modelling and Numerical Analysis
www.esaim-m2an.org

A PWDG METHOD FOR THE MAXWELL SYSTEM IN ANISOTROPIC MEDIA WITH PIECEWISE CONSTANT COEFFICIENT MATRIX

Long Yuan[1,*] and Qiya Hu[2,3,*]

Abstract. In this paper we are concerned with plane wave discontinuous Galerkin (PWDG) methods for time-harmonic Maxwell equations in three-dimensional anisotropic media, for which the coefficients of the equations are piecewise constant symmetric matrices, where each constant symmetric matrix is defined on a medium (subdomain). By using suitable scaling transformations and coordinate (complex) transformations on every subdomain, the original Maxwell equation in anisotropic media is transformed into a Maxwell equation in isotropic media occupying a union domain of specific subdomains of complex Euclidean space. Based on these transformations, we define anisotropic plane wave basis functions and discretize the considered Maxwell equations by PWDG method with the proposed plane wave basis functions. We derive error estimates of the resulting approximate solutions, and further introduce a practically feasible local *hp*-refinement algorithm, which substantially improves accuracies of the approximate solutions. Numerical results indicate that the approximate solutions generated by the proposed PWDG methods possess high accuracy for the case of strong discontinuity media.

Mathematics Subject Classification. 65N30 and 65N55.

Received August 21, 2023. Accepted November 27, 2023.

1. Introduction

The Maxwell equations in anisotropic media with general symmetric matrices play an important role in practical physical applications, for example, determining the response of the inclusion to an impinging acoustic or electromagnetic wave (see the textbooks [6, 14, 16]). Besides, electromagnetic problems within this class also include the design of waveguides and antennas, scattering of electromagnetic waves from automobiles and aircraft, and the penetration and absorption of electromagnetic waves by dielectric objects (see [1–4, 13, 15, 20, 26]). Under this assumption, a permittivity ε and permeability μ can describe a linear metamaterial with no magnetoelectric coupling, where Bianisotropy effects have typically played a minor role in the overall response of the experimental metamaterials, and can be mitigated by design (see [18]).

Keywords and phrases. Time-harmonic Maxwell's equations, anisotropic media, piecewise symmetric matrices, plane wave basis, error estimates.

[1] College of Mathematics and Systems Science, Shandong University of Science and Technology, Qingdao 266590, P.R. China.

[2] LSEC, Institute of Computational Mathematics and Scientic/Engineering Computing, Academy of Mathematics and Systems Science, Chinese Academy of Sciences, Beijing 100190, P.R. China.

[3] School of Mathematical Sciences, University of Chinese Academy of Sciences, Beijing 100049, P.R. China.

*Corresponding author: sdbjbjsd@163.com; hqy@lsec.cc.ac.cn.

The plane wave method, which is based on the Trefftz approximation space made of plane wave basis functions, has a related advantage over Lagrange finite elements for discretization of the time-harmonic Maxwell equations [8]: to achieve the same accuracy, relatively fewer number of degrees of freedom are enough owing to the particular choice of the basis functions that satisfy the considered PDE without boundary conditions. The plane wave method was first introduced to discretization of homogeneous time-harmonic isotropic Maxwell's equations. Various examples of the plane wave methods has been systematically surveyed in [5, 8–11, 17]. Then the plane wave method was extended to discretization of homogeneous anisotropic Maxwell's equations. The work [22] proposed anisotropic plane wave basis functions for the three-dimensional anisotropic Maxwell equations in the particular TE polarization. In addition, the PWDG method was applied to discretization of three-dimensional anisotropic Maxwells equations with simple diagonal matrix coefficients [23], in which rough error estimates of the resulting approximate solutions were derived. Further, the work [24] studied the PWDG method for the time-harmonic Maxwell equations in more general anisotropic media, where the coefficient of the equations is a positive definite constant matrix instead of diagonal matrix. Therein a new assumption on the triangulation was proposed: the transformed triangulation $\hat{\mathcal{T}}_{\hat{h}}$ rather than the physical triangulation $\mathcal{T}_h$ is shape regular, which induces the generation of the anisotropic mesh $\mathcal{T}_h$ and improves the convergence order with respect to the condition number of the coefficient matrix. Although the grid assumption improves the accuracy, it limits the model's applicability only to the case of homogeneous positive definite matrices.

The inhomogeneous anisotropic Maxwell problem is of great difference from the homogeneous anisotropic Maxwell problem. The major difficulty is how to fully capture the interactions among the separate cavities. The study [26] was devoted to computing the mathematical model for the scattering from multiple cavities both in particular TM and TE polarizations, where the cavities are required to be invariant to z-axis, namely, the permittivity ε, and permeability μ, limited to the z-axis, do not interact with other directions.

In the present paper we consider three-dimensional time-harmonic Maxwell equations in more general inhomogeneous anisotropic media, where the coefficient of the equations is a piecewise constant symmetric matrix instead of positive definite matrix. In order to design an efficient numerical method for solving such Maxwell equations, we need to define a scaling transformation and a coordinate transformation on every anisotropic medium (corresponding to a subdomain O_k), in which the coefficient matrix A_k is a constant symmetric matrix, such that the anisotropic medium is transformed into an isotropy medium (corresponding to a subdomain $\hat{O}_k$). As we will see in Section 3 that the coordinate transformation matrix S_k depends on square roots of eigenvalues of the A_k. Since the coefficient matrix A_k is not positive definite, the coordinate transformation matrix S_k are complex matrices, which means that $\hat{O}_k$ is a subdomain of three-dimensional complex Euclidean space. For convenience, we call $\hat{O}_k$ as a complex-valued sub-geometry, where all $\hat{O}_k$ do not intersect each other and may have different sizes. Notice that partitioning all the complex-valued sub-geometry $\hat{O}_k$ is an expensive task, so we still construct a triangulation $\mathcal{T}_{h_k^s}$ on the original subdomain O_k as usual and then generate a *virtual* triangulation $\hat{\mathcal{T}}_{\hat{h}_k^s}$ on $\hat{O}_k$. Based on these transformations, we define anisotropic plane wave basis functions and discretize the considered Maxwell equations by PWDG method with the proposed plane wave basis functions. We prove the stability estimates of the transformations on the condition number of the piecewise constant anisotropic matrices, and further prove the error estimates of the resulting approximate solutions.

In order to improve the accuracies of the approximate solutions, we introduce a practically feasible local hp-refinement algorithm. For p-refinement, the number of basis functions p_k employed in the subdomain O_k is adaptive to the diameter of the artificial sub-geometry $\hat{O}_k$ rather than that of the original subdomain O_k, namely, $p_k \propto \hat{H}_k = \mathrm{diam}(\hat{O}_k)$. Then, for h-refinement, according to the ascending order of the diameters of the artificial sub-geometries $\{\hat{O}_k\}$, the diameter of the triangulation $\mathcal{T}_{h_k^s}$ of each subdomain O_k satisfies that $h_1^s \approx \mathcal{O}(\frac{\hat{h}}{\hat{H}_1}) \geq h_2^s \approx \mathcal{O}(\frac{\hat{h}}{\hat{H}_2}) \geq h_3^s \approx \mathcal{O}(\frac{\hat{h}}{\hat{H}_3}) \geq \cdots$ in a proper way. Numerical experiments indicate that, for the case of strong discontinuity media, the usage of feasible local hp-refinement algorithm substantially improves the resulting approximate accuracy.

We would like to emphasize the difference between the PWDG method proposed in this paper for inhomogeneous anisotropic media (with a piecewise constant symmetric coefficient matrix) and the PWDG method in

[24] for homogeneous anisotropic media (with a positive definite efficient matrix). For both the two methods, the triangulations made on non physical region $\hat{\Omega}$ must meet the shape regular assumption, but their implementation processes are completely different. For the case of homogeneous anisotropic media with the positive definite matrix, $\hat{\Omega}$ is directly decomposed into polyhedron elements $\{\hat{\Omega}_k\}$ such that $\hat{\mathcal{T}}_{\hat{h}}$ is shape regular. While for the current situation, since the generated domain $\hat{\Omega}$ is a complex-valued region, we partition the original domain Ω to generate a realistic triangulation $\mathcal{T}_h$ and then obtain a virtual triangulation $\hat{\mathcal{T}}_{\hat{h}}$ on $\{\hat{\Omega}_k\}$, where the shape regular assumption can be satisfied too thanking to the proposed local hp-refinement algorithm.

The paper is organized as follows. In Section 2, we give the first-order 3D system of inhomogeneous Maxwell equations and its variational formula associated with triangulation. In Section 3, we present the anisotropic plane wave discretization for the inhomogeneous Maxwell equations. In Section 4, we give error estimates for the approximate solutions. In Section 5, we further propose the local hp-refinement algorithm. Finally, we report some numerical results to confirm the effectiveness of the proposed method.

2. The model and its variational formula

We consider the inhomogeneous anisotropic time-harmonic Maxwell equations written as a first-order system of equations:

$$\begin{cases} \nabla \times \mathbf{E} - i\omega\mu\mathbf{H} = \mathbf{0} \\ \nabla \times \mathbf{H} + i\omega\varepsilon\mathbf{E} = \mathbf{0} \\ \nabla \cdot (\varepsilon\mathbf{E}) = 0 \\ \nabla \cdot (\mu\mathbf{H}) = 0 \end{cases} \quad \text{in} \quad \Omega \tag{2.1}$$

with the lowest-order absorbing boundary condition

$$\mathbf{H} \times \mathbf{n} - \vartheta(\mathbf{n} \times \mathbf{E}) \times \mathbf{n} = \mathbf{g}/i\omega \quad \text{on} \quad \gamma = \partial\Omega. \tag{2.2}$$

Here $\mathbf{E} = (E_x, E_y, E_z)^T$, $\mathbf{H} = (H_x, H_y, H_z)^T$, i is the imaginary unit, $\omega > 0$ is the temporal frequency of the field, $\vartheta > 0$ is assumed to be constant, $\mathbf{n}$ is the outer normal unit vector to $\partial\Omega$ and $\mathbf{g} \in \mathbf{L}^2(\partial\Omega)$. The permittivity ε and the permeability μ are assumed to be of the form $\varepsilon = \varepsilon_r A$, $\mu = \mu_r A$, where $\varepsilon_r, \mu_r \in \mathbb{R}$ are piecewise nonzero constants, and A is a 3×3 piecewise constant matrix satisfying symmetry and reversibility.

By eliminating $\mathbf{H}$ from (2.1) and (2.2), we obtain the second-order inhomogeneous anisotropic Maxwell equations of $\mathbf{E}$:

$$\begin{cases} \nabla \times \left(\mu^{-1}\nabla \times \mathbf{E}\right) - \omega^2\varepsilon\mathbf{E} = 0 & \text{in} \quad \Omega, \\ \dfrac{1}{i\omega}\mu^{-1}\nabla \times \mathbf{E} \times \mathbf{n} - \vartheta(\mathbf{n} \times \mathbf{E}) \times \mathbf{n} = \mathbf{g}/i\omega & \text{on} \quad \gamma. \end{cases} \tag{2.3}$$

We will derive a variational formula of (2.1) based on a partition of the solution domain Ω (refer to [8, 24]).

For convenience, assume that Ω is a polyhedron. Let Ω be partitioned into a union of some elements in the sense that

$$\overline{\Omega} = \bigcup_{k=1}^{N} \overline{\Omega}_k, \quad \Omega_l \bigcap \Omega_j = \emptyset \quad \text{for } l \neq j,$$

where each Ω_k is a polyhedron. Let $\mathcal{T}_h$ denote the mesh comprised of the elements $\{\Omega_k\}$, where h_k denotes the diameter of the element Ω_k, and h denotes the global mesh size $h = \max_{\Omega_k \in \mathcal{T}_h} h_k$. Define

$$\Gamma_{lj} = \partial\Omega_l \bigcap \partial\Omega_j, \quad \text{for } l \neq j$$

and

$$\gamma_k = \overline{\Omega}_k \bigcap \partial\Omega \quad (k = 1, \ldots, N), \quad \gamma = \bigcup_{k=1}^{N} \gamma_k.$$

We denote by $\mathcal{F}_h = \bigcup_k \partial\Omega_k$ the skeleton of the mesh, and set $\mathcal{F}_h^{\mathrm{B}} = \mathcal{F}_h \bigcap \partial\Omega$ and $\mathcal{F}_h^{\mathrm{I}} = \mathcal{F}_h \backslash \mathcal{F}_h^{\mathrm{B}}$. Let $\boldsymbol{\sigma}$ be a piecewise smooth vector field on $\mathcal{T}_h$. On $\partial\Omega_l \bigcap \partial\Omega_j$, we define

$$\begin{aligned} \text{the average: } \{\{\boldsymbol{\sigma}\}\} &:= \frac{\boldsymbol{\sigma}_l + \boldsymbol{\sigma}_j}{2}, \\ \text{the tangential jump: } [\![\boldsymbol{\sigma}]\!]_T &:= \mathbf{n}_l \times \boldsymbol{\sigma}_l + \mathbf{n}_j \times \boldsymbol{\sigma}_j, \end{aligned} \tag{2.4}$$

where $\mathbf{n}_k$ denotes a unit outer normal vector on the boundary of the element Ω_k. We assume that the mesh $\mathcal{T}_h$ is chosen such that ε_r, μ_r, and the anisotropic matrix A are constant on each element Ω_k. Further, we set $\Box|_{\Omega_k} = \Box_k$, where $\Box$ denote ε, μ, A and $\varepsilon_{r,}, \mu_{r,}$, respectively.

Define the broken Sobolev space

$$\mathbf{H}^r(\mathrm{curl}; \mathcal{T}_h) = \{\mathbf{w} \in \mathbf{L}^2(\Omega) : \mathbf{w}|_{\Omega_k} \in \mathbf{H}^r(\mathrm{curl}; \Omega_k), \quad \forall \Omega_k \in \mathcal{T}_h\}. \tag{2.5}$$

Let $\mathbf{V}(\mathcal{T}_h)$ be the piecewise Trefftz space defined on $\mathcal{T}_h$ by

$$\begin{aligned} \mathbf{V}(\mathcal{T}_h) = \Big\{ &\mathbf{w} \in \mathbf{L}^2(\Omega) : \exists s > 0 \text{ s.t. } \mathbf{w} \in \mathbf{H}^{1/2+s}(\mathrm{curl}; \mathcal{T}_h), \\ &\text{and } \nabla \times (\mu^{-1} \nabla \times \mathbf{w}) - \omega^2 \varepsilon \mathbf{w} = \mathbf{0} \text{ in } \quad \text{each } \ \Omega_k \in \mathcal{T}_h \Big\}. \end{aligned} \tag{2.6}$$

Let α, β, δ be strictly positive constants, with $0 < \delta \leq 1/2$. As in Section 3 of [8], define the sesquilinear form $\mathcal{A}_h(\cdot,\cdot)$ by

$$\begin{aligned} \mathcal{A}_h(\mathbf{E}, \boldsymbol{\xi}) = &- \int_{\mathcal{F}_h^{\mathrm{I}}} \{\{\mathbf{E}\}\} \cdot \overline{[\![\mu^{-1} \nabla_h \times \boldsymbol{\xi}]\!]_T} \, \mathrm{d}S - i\omega^{-1} \int_{\mathcal{F}_h^{\mathrm{I}}} \beta [\![\mu^{-1} \nabla_h \times \mathbf{E}]\!]_T \cdot \overline{[\![\mu^{-1} \nabla_h \times \boldsymbol{\xi}]\!]_T} \, \mathrm{d}S \\ &- \int_{\mathcal{F}_h^{\mathrm{I}}} \big\{\{\mu^{-1} \nabla_h \times \mathbf{E}\}\big\} \cdot \overline{[\![\boldsymbol{\xi}]\!]_T} \, \mathrm{d}S - i\omega \int_{\mathcal{F}_h^{\mathrm{I}}} \alpha [\![\mathbf{E}]\!]_T \cdot \overline{[\![\boldsymbol{\xi}]\!]_T} \, \mathrm{d}S \\ &+ \int_{\mathcal{F}_h^{\mathrm{B}}} (1-\delta)(\mathbf{n} \times \mathbf{E}) \cdot \overline{(\mu^{-1} \nabla_h \times \boldsymbol{\xi})} \, \mathrm{d}S - \int_{\mathcal{F}_h^{\mathrm{B}}} \delta \big(\mu^{-1} \nabla_h \times \mathbf{E}\big) \cdot \overline{(\mathbf{n} \times \boldsymbol{\xi})} \, \mathrm{d}S \\ &- i\omega^{-1} \int_{\mathcal{F}_h^{\mathrm{B}}} \delta \vartheta^{-1} \big[\mathbf{n} \times \big(\mu^{-1} \nabla_h \times \mathbf{E}\big)\big] \cdot \overline{[\mathbf{n} \times (\mu^{-1} \nabla_h \times \boldsymbol{\xi})]} \, \mathrm{d}S \\ &- i\omega \int_{\mathcal{F}_h^{\mathrm{B}}} (1-\delta) \vartheta (\mathbf{n} \times \mathbf{E}) \cdot \overline{(\mathbf{n} \times \boldsymbol{\xi})} \, \mathrm{d}S, \qquad \forall \boldsymbol{\xi} \in \mathbf{V}(\mathcal{T}_h) \end{aligned}$$

and the functional $\ell_h(\cdot,\cdot)$ by

$$\ell_h(\mathbf{g}, \boldsymbol{\xi}) = -i\omega^{-1} \int_{\mathcal{F}_h^{\mathrm{B}}} \delta \vartheta^{-1} (\mathbf{n} \times \mathbf{g}) \cdot \overline{\mu^{-1} \nabla_h \times \boldsymbol{\xi}} \, \mathrm{d}S + \int_{\mathcal{F}_h^{\mathrm{B}}} (1-\delta)(\mathbf{n} \times \mathbf{g}) \cdot \overline{(\mathbf{n} \times \boldsymbol{\xi})} \, \mathrm{d}S, \qquad \forall \boldsymbol{\xi} \in \mathbf{V}(\mathcal{T}_h) \tag{2.7}$$

Then, for a given $\mathbf{g}$, the variational problem associated with (2.1) can be expressed as follows (see [8], Sect. 3). Find $\mathbf{E} \in \mathbf{V}(\mathcal{T}_h)$ such that,

$$\mathcal{A}_h(\mathbf{E}, \boldsymbol{\xi}) = \ell_h(\mathbf{g}, \boldsymbol{\xi}), \qquad \forall \boldsymbol{\xi} \in \mathbf{V}(\mathcal{T}_h). \tag{2.8}$$

Remark 2.1. This choice of the so-called flux parameters α, β, δ independent of the mesh size h, the number p of basis functions on each element and the material coefficients, is due to the fact that, as stated below, the proposed scaled transformation and coordinate transformation transfer the anisotropy of the original equation to the isotropy defined in the specially artificial sub-geometries with different sizes that do not intersect with each other, which motivates us to develop a local *hp*-refinement algorithm to improve the resulting approximate accuracy without considering the contribution of flux parameters. In the future, we will consider the contribution of variable flux parameters to the error estimates.

3. Anisotropic plane wave discretization for the inhomogeneous Maxwell equations

In this section, we introduce an anisotropic plane wave discretization for (2.8). The proposed plane wave method for (2.1) depends on two transformations. By using suitable scaling transformations and coordinate (complex) transformations on every subdomain, which are different from that proposed in [24] on the whole domain, the original Maxwell equation in anisotropic media is transformed into a Maxwell equation in isotropic media occupying a union domain of specific subdomains of complex Euclidean space.

3.1. Two different types of scaled transformations and coordinate transformations

Since A is the real-valued symmetric matrix on each element Ω_k, there exists an orthogonal matrix P_k and a diagonal matrix $\Lambda_k = \mathrm{diag}(\lambda_1^{(k)}, \lambda_2^{(k)}, \lambda_3^{(k)})$ such that $A_k = A|_{\Omega_k} = P_k^T \Lambda_k P_k$, where $\lambda_1^{(k)}, \lambda_2^{(k)}, \lambda_3^{(k)}$ are real-valued constants. Of course, we can assume that $\det(P_k) = 1$. In particular, $\lambda_1^{(k)}, \lambda_2^{(k)}, \lambda_3^{(k)}$ satisfy the ascending order by modulus: $|\lambda_1^{(k)}| \le |\lambda_2^{(k)}| \le |\lambda_3^{(k)}|$, and for readability, we set $\lambda_{\min}^{(k)} = \lambda_1^{(k)}, \lambda_{\mathrm{mid}}^{(k)} = \lambda_2^{(k)}, \lambda_{\max}^{(k)} = \lambda_3^{(k)}$. Furthermore, we construct a set of data

$$m_{\max}^{(k)} = \sqrt{\lambda_{\mathrm{mid}}^{(k)} \lambda_{\max}^{(k)}}, \quad m_{\mathrm{mid}}^{(k)} = \sqrt{\lambda_{\max}^{(k)} \lambda_{\min}^{(k)}} \quad \text{and} \quad m_{\min}^{(k)} = \sqrt{\lambda_{\min}^{(k)} \lambda_{\mathrm{mid}}^{(k)}}. \tag{3.1}$$

Note that $m_{\max}^{(k)}, m_{\mathrm{mid}}^{(k)}$ and $m_{\min}^{(k)}$ may be *complex*-valued.

For convenience, we use $\mathbf{p}_1^{(k)}, \mathbf{p}_2^{(k)}$ and $\mathbf{p}_3^{(k)}$ to denote the three column vectors of P_k, and use $(\mathbf{q}_1^{(k)})^T, (\mathbf{q}_2^{(k)})^T, (\mathbf{q}_3^{(k)})^T$ to denote the three row vectors of P_k. Then $\mathbf{p}_1^{(k)}, \mathbf{p}_2^{(k)}$ and $\mathbf{p}_3^{(k)}$ (and $\mathbf{q}_1^{(k)}, \mathbf{q}_2^{(k)}, \mathbf{q}_3^{(k)}$) are three dimensional unit vectors that are orthogonal to each other.

Define the scaled fields $\tilde{\mathbf{E}}$ and $\tilde{\mathbf{H}}$ on each element Ω_k as

$$\begin{aligned} (E_x, E_y, E_z)^T &= G_k \Big(\tilde{E}_x, \tilde{E}_y, \tilde{E}_z\Big)^T, \\ (H_x, H_y, H_z)^T &= G_k \Big(\tilde{H}_x, \tilde{H}_y, \tilde{H}_z\Big)^T. \end{aligned} \tag{3.2}$$

Here $G_k = P_k^T \Lambda_k^{-\frac{1}{2}}$. Note that $\Lambda_k^{-\frac{1}{2}} = \mathrm{diag}((\lambda_{\min}^{(k)})^{-\frac{1}{2}}, (\lambda_{\mathrm{mid}}^{(k)})^{-\frac{1}{2}}, (\lambda_{\max}^{(k)})^{-\frac{1}{2}})$, whose element on the diagonal may be *complex*-valued.

Without causing confusion, we omit the usage of subscript k and superscript (k), which is a limitation of anisotropic objects on each element Ω_k. Then, by direct calculation and (3.2), we have, on each element,

$$\begin{aligned} \nabla \times \mathbf{E} &= P^T \Lambda^{\frac{1}{2}} \left(-\frac{\mathbf{q}_3 \cdot \nabla \tilde{E}_y}{m_{\min}} + \frac{\mathbf{q}_2 \cdot \nabla \tilde{E}_z}{m_{\mathrm{mid}}}, \frac{\mathbf{q}_3 \cdot \nabla \tilde{E}_x}{m_{\min}} - \frac{\mathbf{q}_1 \cdot \nabla \tilde{E}_z}{m_{\max}}, -\frac{\mathbf{q}_2 \cdot \nabla \tilde{E}_x}{m_{\mathrm{mid}}} + \frac{\mathbf{q}_1 \cdot \nabla \tilde{E}_y}{m_{\max}} \right)^T, \\ \nabla \times \mathbf{H} &= P^T \Lambda^{\frac{1}{2}} \left(-\frac{\mathbf{q}_3 \cdot \nabla \tilde{H}_y}{m_{\min}} + \frac{\mathbf{q}_2 \cdot \nabla \tilde{H}_z}{m_{\mathrm{mid}}}, \frac{\mathbf{q}_3 \cdot \nabla \tilde{H}_x}{m_{\min}} - \frac{\mathbf{q}_1 \cdot \nabla \tilde{H}_z}{m_{\max}}, -\frac{\mathbf{q}_2 \cdot \nabla \tilde{H}_x}{m_{\mathrm{mid}}} + \frac{\mathbf{q}_1 \cdot \nabla \tilde{H}_y}{m_{\max}} \right)^T, \\ \mu \mathbf{H} &= \mu_r P^T \Lambda P P^T \Lambda^{-\frac{1}{2}} \tilde{\mathbf{H}} = \mu_r P^T \Lambda^{\frac{1}{2}} \tilde{\mathbf{H}}, \\ \varepsilon \mathbf{E} &= \varepsilon_r P^T \Lambda P P^T \Lambda^{-\frac{1}{2}} \tilde{\mathbf{E}} = \varepsilon_r P^T \Lambda^{\frac{1}{2}} \tilde{\mathbf{E}}. \end{aligned} \tag{3.3}$$

Here, we give the simple derivation of the second equation of (3.3), the remaining three equations can be obtained in a similar way. For the sake of clarity, we rewrite $\tilde{\mathbf{H}}$ as $\tilde{\mathbf{H}} = (\tilde{H}_1, \tilde{H}_2, \tilde{H}_3)^T$ and $(m_{\min}, m_{\mathrm{mid}}, m_{\max})$ as (m_1, m_2, m_3). Then by (3.2), $\nabla \times (\mathbf{a}u) = \nabla u \times \mathbf{a}$ (for any constant vector $\mathbf{a} \in \mathbb{C}^3$), an orthogonal matrix P satisfying $(P^T)^* = (P^T)^T$, where $\square^*$ denote the adjoint matrix of $\square$, and $\det(P) = 1$, we have

$$\nabla \times \mathbf{H} = \sum_{i=1}^{3} \lambda_i^{-\frac{1}{2}} \nabla \tilde{H}_i \times \mathbf{q}_i = \lambda_1^{-\frac{1}{2}} \Big(\mathbf{q}_2 \Big(\mathbf{q}_3 \cdot \nabla \tilde{H}_1 \Big) - \mathbf{q}_3 \Big(\mathbf{q}_2 \cdot \nabla \tilde{H}_1 \Big) \Big)$$

$$
\begin{aligned}
&+\lambda_2^{-\frac{1}{2}}\Big(\mathbf{q}_3\Big(\mathbf{q}_1\cdot\nabla\tilde{H}_2\Big)-\mathbf{q}_1\Big(\mathbf{q}_3\cdot\nabla\tilde{H}_2\Big)\Big)+\lambda_3^{-\frac{1}{2}}\Big(\mathbf{q}_1\Big(\mathbf{q}_2\cdot\nabla\tilde{H}_3\Big)-\mathbf{q}_2\Big(\mathbf{q}_1\cdot\nabla\tilde{H}_3\Big)\Big)\\
=&\,\mathbf{q}_1\Big(-\lambda_2^{-\frac{1}{2}}\mathbf{q}_3\cdot\nabla\tilde{H}_2+\lambda_3^{-\frac{1}{2}}\mathbf{q}_2\cdot\nabla\tilde{H}_3\Big)+\mathbf{q}_2\Big(\lambda_1^{-\frac{1}{2}}\mathbf{q}_3\cdot\nabla\tilde{H}_1-\lambda_3^{-\frac{1}{2}}\mathbf{q}_1\cdot\nabla\tilde{H}_3\Big)\\
&+\mathbf{q}_3\Big(-\lambda_1^{-\frac{1}{2}}\mathbf{q}_2\cdot\nabla\tilde{H}_1+\lambda_2^{-\frac{1}{2}}\mathbf{q}_1\cdot\nabla\tilde{H}_2\Big)\\
=&\,P^T\Lambda^{\frac{1}{2}}\left(-\frac{\mathbf{q}_3\cdot\nabla\tilde{H}_2}{m_1}+\frac{\mathbf{q}_2\cdot\nabla\tilde{H}_3}{m_2},\frac{\mathbf{q}_3\cdot\nabla\tilde{H}_1}{m_1}-\frac{\mathbf{q}_1\cdot\nabla\tilde{H}_3}{m_3},-\frac{\mathbf{q}_2\cdot\nabla\tilde{H}_1}{m_2}+\frac{\mathbf{q}_1\cdot\nabla\tilde{H}_2}{m_3}\right)^T.
\end{aligned}
\tag{3.4}
$$

Set $M=\mathrm{diag}(m_{\max},m_{\mathrm{mid}},m_{\min})$, and define the coordinate transformation

$$
\hat{\mathbf{x}}=(\hat{x}\ \hat{y}\ \hat{z})^T=\ M\ P\ (x\ y\ z)^T\overset{\Delta}{=\!=}S\ \mathbf{x},\quad S=M\ P. \tag{3.5}
$$

With the inverse transformation S^{-1}, we define the scaled electric and magnetic fields

$$
\Big(\hat{\mathbf{E}}(\hat{\mathbf{x}}),\hat{\mathbf{H}}(\hat{\mathbf{x}})\Big)^T=\Big(\tilde{\mathbf{E}}\big(S^{-1}\hat{\mathbf{x}}\big),\tilde{\mathbf{H}}\big(S^{-1}\hat{\mathbf{x}}\big)\Big)^T. \tag{3.6}
$$

By (3.5) and (3.6) and direct manipulation, the righthands of (3.3) can be reduced to the following system (The divergence operators are applied to the last two terms)

$$
\begin{aligned}
\left(-\frac{\mathbf{q}_3\cdot\nabla\tilde{E}_y}{m_{\min}}+\frac{\mathbf{q}_2\cdot\nabla\tilde{E}_z}{m_{\mathrm{mid}}},\frac{\mathbf{q}_3\cdot\nabla\tilde{E}_x}{m_{\min}}-\frac{\mathbf{q}_1\cdot\nabla\tilde{E}_z}{m_{\max}},-\frac{\mathbf{q}_2\cdot\nabla\tilde{E}_x}{m_{\mathrm{mid}}}+\frac{\mathbf{q}_1\cdot\nabla\tilde{E}_y}{m_{\max}}\right)^T&=\hat{\nabla}\times\hat{\mathbf{E}},\\
\left(-\frac{\mathbf{q}_3\cdot\nabla\tilde{H}_y}{m_{\min}}+\frac{\mathbf{q}_2\cdot\nabla\tilde{H}_z}{m_{\mathrm{mid}}},\frac{\mathbf{q}_3\cdot\nabla\tilde{H}_x}{m_{\min}}-\frac{\mathbf{q}_1\cdot\nabla\tilde{H}_z}{m_{\max}},-\frac{\mathbf{q}_2\cdot\nabla\tilde{H}_x}{m_{\mathrm{mid}}}+\frac{\mathbf{q}_1\cdot\nabla\tilde{H}_y}{m_{\max}}\right)^T&=\hat{\nabla}\times\hat{\mathbf{H}},\\
\nabla\cdot\Big(P^T\Lambda^{\frac{1}{2}}\tilde{\mathbf{H}}\Big)&=M\Lambda^{\frac{1}{2}}\hat{\nabla}\cdot\hat{\mathbf{H}},\\
\nabla\cdot\Big(P^T\Lambda^{\frac{1}{2}}\tilde{\mathbf{E}}\Big)&=M\Lambda^{\frac{1}{2}}\hat{\nabla}\cdot\hat{\mathbf{E}}.
\end{aligned}
\tag{3.7}
$$

Thus, by (2.1), (3.3) and (3.6), (3.7), the scaled electric and magnetic fields $(\hat{\mathbf{E}}(\hat{\mathbf{x}}),\hat{\mathbf{H}}(\hat{\mathbf{x}}))$ satisfy the transformed isotropic Maxwell equations:

$$
\begin{cases}
\hat{\nabla}\times\hat{\mathbf{E}}-i\omega\mu_r\hat{\mathbf{H}}=\mathbf{0}\\
\hat{\nabla}\times\hat{\mathbf{H}}+i\omega\varepsilon_r\hat{\mathbf{E}}=\mathbf{0}\\
\hat{\nabla}\cdot\Big(\varepsilon_r\hat{\mathbf{E}}\Big)=0\\
\hat{\nabla}\cdot\Big(\mu_r\hat{\mathbf{H}}\Big)=0
\end{cases}
\quad\text{in}\quad\hat{\Omega}. \tag{3.8}
$$

Conversely, if the scaled electric and magnetic fields $(\hat{\mathbf{E}}(\hat{\mathbf{x}}),\hat{\mathbf{H}}(\hat{\mathbf{x}}))$ satisfy the transformed isotropic Maxwell equations (3.8), the physical electromagnetic fields $\big(\mathbf{E}(\mathbf{x}),\mathbf{H}(\mathbf{x})\big)$

$$
\begin{cases}
\mathbf{E}(\mathbf{x})=G\hat{\mathbf{E}}(\hat{\mathbf{x}})=G\hat{\mathbf{E}}(S\mathbf{x})\\
\mathbf{H}(\mathbf{x})=G\hat{\mathbf{H}}(\hat{\mathbf{x}})=G\hat{\mathbf{H}}(S\mathbf{x})
\end{cases} \tag{3.9}
$$

satisfy the original anisotropic Maxwell equations (2.1).

Let $\hat{\Omega}$ and $\hat{\Omega}_k$ denote the images of Ω and Ω_k under the coordinate transformation (3.5), respectively. Since the map S is linear, the transformed domain $\hat{\Omega}$ and elements $\hat{\Omega}_k$ are also polyhedrons. We use $\hat{\mathbf{n}}_k$ to denote the unit outer normal vector on the boundary of each element $\hat{\Omega}_k$, and $\hat{\mathcal{T}}_{\hat{h}}$ to denote the partition comprised by the elements $\{\hat{\Omega}_k\}$, where $\hat{h}$ is the maximal diameter of the transformed elements $\{\hat{\Omega}_k\}$. Set $\hat{\mathcal{F}}_{\hat{h}}=\bigcup_k\partial\hat{\Omega}_k$.

Remark 3.1. Suppose that Ω is divided into several subdomains $\{O_k\}$, and further that the anisotropic matrix A is constant on each subdomain. We point out that, the transformed *sub-geometries* $\{\hat{O}_k\}$ of the subdomains $\{O_k\}$ may not be connected to each other; namely, $\partial\hat{O}_k \bigcap \partial\hat{O}_j = \emptyset$ when $k \neq j$. Moreover, the existence of discontinuous media may lead to marked differences in the shape and size of different sub-geometries.

Remark 3.2. Since the transformation matrix S in (3.5) may take complex values when the anisotropic matrix A is symmetric not positively definite, the corresponding transformed domain $\hat{\Omega}$ must be a complex-valued region. As we all know that partitioning the complex-valued domain is an expensive task. Fortunately, we just need the *virtual* mesh partition $\hat{\mathcal{T}}_{\hat{h}}$ of $\hat{\Omega}$ to achieve the transformation stability estimates and the error estimates to be proven below, rather than implementing partitioning on the transformed domain.

We would like to point out that, the option of the scaled transformation (3.2) and the coordinate transformation (3.5) is *not unique*. On the one hand, for the choice of $G = P\Lambda^{-\frac{1}{2}}$ and $S = MP$, the orthogonal matrix P associated with the eigenvectors of the symmetric matrix A cannot be uniquely determined. On the other hand, if the scaled matrix G and coordinated matrix S are chosen in another way: $G = P^T\Lambda^{-\frac{1}{2}}P$ and $S = P^TMP$, then the original anisotropic Maxwell equations (2.1) and the transformed isotropic Maxwell equations (3.8) can be equivalently derived from each other. Although the choice of the transformation are diverse, they do not affect the stability estimate (4.13) and error estimate (4.29) later proved, owing to the nice properties of orthogonal matrix P such as $\|P\| = 1$ and preserving geometric structure.

In the next subsection we present an anisotropic plane wave discretization method for the considered inhomogeneous Maxwell equations by using the scaling matrix (3.2) and the coordinate transformation (3.5).

3.2. Anisotropic plane wave basis function spaces

The discretization of the PWDG method is based on a finite-dimensional anisotropic plane wave subspace $\mathbf{V}_p(\mathcal{T}_h) \subset \mathbf{V}(\mathcal{T}_h)$. We first define plane wave basis function space $\hat{\mathbf{V}}_p(\hat{\mathcal{T}}_{\hat{h}})$ satisfying the isotropic Maxwell equations (3.8).

By choosing p unit propagation directions $\mathbf{d}_l$ $(l = 1, \cdots, p)$, which can be determined by the codes in [21], we then define isotropic plane wave basis functions $\hat{\mathbf{E}}_l$:

$$\hat{\mathbf{E}}_l = \mathbf{F}_l \exp(\mathrm{i}\ \kappa\ \mathbf{d}_l \cdot \hat{\mathbf{x}}) \quad \text{and} \quad \hat{\mathbf{E}}_{l+p} = \mathbf{G}_l \exp(\mathrm{i}\ \kappa\ \mathbf{d}_l \cdot \hat{\mathbf{x}}) \quad (l = 1, \cdots, p), \tag{3.10}$$

where $\kappa = \omega\sqrt{\mu_r\varepsilon_r}$, $\mathbf{F}_l$ and $\mathbf{G}_l$ are polarization vectors satisfying $\mathbf{F}_l \cdot \mathbf{d}_l = 0$ and $\mathbf{G}_l = \mathbf{F}_l \times \mathbf{d}_l$ $(l = 1, \cdots, p)$.

We point out that the choices of unit wave propagation directions are not unique and other plane wave propagation directions work as well, such as the directions based on spherical coordinates (see [12]). Besides, the propagation directions can be trained by the discontinuous plane wave neural networks for iteratively solving the minimization problem associated with the underlying residual functionals (see [25]).

Choose the number p of plane wave propagation directions as $p = (m+1)^2$, where m is a positive integer. Let $\hat{\mathcal{Q}}_{2p}$ denote the discrete space spanned by the $2p$ plane wave basis functions $\hat{\mathbf{E}}_l$ $(l = 1, \cdots, 2p)$, and define the isotropic plane wave discrete space

$$\hat{\mathbf{V}}_p(\hat{\mathcal{T}}_{\hat{h}}) = \left\{ \hat{\mathbf{v}} \in \mathbf{L}^2(\Omega) : \ \hat{\mathbf{v}}|_{\hat{K}} \in \hat{\mathcal{Q}}_{2p} \ \text{ for any } \ \hat{K} \in \hat{\mathcal{T}}_{\hat{h}} \right\}. \tag{3.11}$$

By the transformations (3.9), we are able to define the anisotropic plane wave basis functions satisfying the original equations (2.1):

$$\mathbf{E}_l = \ G\ \mathbf{F}_l \exp(\mathrm{i}\ \kappa\ \mathbf{d}_l \cdot S\mathbf{x}) \quad \text{and} \quad \mathbf{E}_{l+p} = \ G\ \mathbf{G}_l \exp(\mathrm{i}\ \kappa\ \mathbf{d}_l \cdot S\mathbf{x}) \quad (l = 1, \cdots, p). \tag{3.12}$$

Let $\mathcal{Q}_{2p}$ denote the anisotropic discrete space spanned by the $2p$ plane wave basis functions $\mathbf{E}_l$ $(l = 1, \cdots, 2p)$, and define the anisotropic plane wave discrete space

$$\mathbf{V}_p(\mathcal{T}_h) = \left\{ \mathbf{v} \in \mathbf{L}^2(\Omega) : \ \mathbf{v}|_K \in \mathcal{Q}_{2p} \ \text{ for any } \ K \in \mathcal{T}_h \right\}. \tag{3.13}$$

It is apparent that the above discrete space has $N \times 2p$ discontinuous basis functions, which are defined by

$$\boldsymbol{\phi}_l^k(\mathbf{x}) = \begin{cases} \mathbf{E}_l(\mathbf{x}), & \mathbf{x} \in \Omega_k, \\ 0, & \mathbf{x} \in \Omega_j \ \text{ satisfying } \ j \neq k \end{cases} \quad (k, j = 1, \cdots, N;\ l = 1, \cdots, 2p). \tag{3.14}$$

Thus, for a given boundary term $\mathbf{g}$, we obtain the discretized PWDG version of the continuous variational problem (2.8): Find $\mathbf{E}_h \in \mathbf{V}_p(\mathcal{T}_h)$ such that,

$$\mathcal{A}_h(\mathbf{E}_h, \boldsymbol{\xi}_h) = \ell_h(\mathbf{g}, \boldsymbol{\xi}_h), \quad \forall \boldsymbol{\xi}_h \in \mathbf{V}_p(\mathcal{T}_h). \tag{3.15}$$

For convenience, we use $\hat{\mathbf{V}}(\hat{\mathcal{T}}_{\hat{h}})$ to denote the image space of the space $\mathbf{V}(\mathcal{T}_h)$ under the scaling transformation (3.2) and the coordinate transformation (3.5), and set $\hat{\mathbf{E}}_{\hat{h}}(\hat{\mathbf{x}}) = G^{-1}\mathbf{E}_h(S^{-1}\hat{\mathbf{x}})$.

4. Error estimates of the approximate solutions

In this section, we are devoted to the analysis of convergence of the plane wave approximation $\mathbf{E}_h$.

4.1. Geometric properties

In order to derive the error estimates of the approximate solutions, we require that the conforming mesh $\mathcal{T}_h$ must satisfy shape regular assumption in the usual manner.

For a 3×3 complex-valued matrix $B \in \mathbb{C}^{3\times 3}$, we define

$$\|B\| = \|B\|_2 = \max_{\mathbf{0} \neq \mathbf{x} \in \mathbb{C}^3} \frac{\|B\mathbf{x}\|_2}{\|\mathbf{x}\|_2}, \tag{4.1}$$

where $\mathbf{x} = (x_1, x_2, x_3)^T$ and $\|\mathbf{x}\|_2 = (|x_1|^2 + |x_2|^2 + |x_3|^2)^{\frac{1}{2}}$. For the simplicity of notation, let ρ_k denote the condition number $\mathrm{cond}(A_k)$ of the anisotropic matrix A_k. Then it is well known that $\rho_k = \mathrm{cond}(\Lambda_k) = \mathrm{cond}^2(\Lambda_k^{\frac{1}{2}}) = \mathrm{cond}^2(S_k) = \mathrm{cond}^2(M_k)$.

The next lemma gives a geometric relation between the meshsizes of two triangulations.

Lemma 4.1. *For the proposed triangulation, we have*

$$\hat{h} \leq \left(\max_k \|M_k\|\right) h \stackrel{\Delta}{=\!=} C_1 h. \tag{4.2}$$

Proof. By the coordinate transformation (3.5) and the definition of matrix norm, we get the result. □

The next lemma gives a relation between the areas of two bounded planes based on the coordinate transformation (3.5).

Lemma 4.2. *For the proposed triangulation, denote by Γ a triangle in 3D which belongs to $\mathcal{F}_h \bigcap \partial\Omega_k$, and by $\hat{\Gamma}$ the correspondingly transformed complex Euclidean triangle which belongs to $\hat{\mathcal{F}}_{\hat{h}} \bigcap \partial\hat{\Omega}_k$. Then we have*

$$\frac{|\Gamma|}{|\hat{\Gamma}|} \leq \left|m_{\mathrm{mid}}^{(k)}\right|^{-1} \left|m_{\mathrm{min}}^{(k)}\right|^{-1}, \tag{4.3}$$

where $|f|$ denotes the area of a bounded plane f in the three-dimensional space, and $|\Box|$ denotes the module of complex quantity $\Box$.

Proof. For simplicity, we omit the usage of subscript k and superscript (k), which is a limitation of anisotropic objects on each element Ω_k. In order to achieve the coordinate transformation (3.5), we define two sub-transformation $\tilde{\mathbf{x}} = P\mathbf{x}$ and $\hat{\mathbf{x}} = M\tilde{\mathbf{x}}$. Since the orthogonal transformation $\tilde{\mathbf{x}} = P\mathbf{x}$ does not change the angle between vectors and the length of vectors, we only need to prove the desired result under the sub-transformation $\hat{\mathbf{x}} = (\hat{x}\ \hat{y}\ \hat{z})^T = M\tilde{\mathbf{x}} = M(\tilde{x}\ \tilde{y}\ \tilde{z})^T$, which is, namely,

$$\tilde{\mathbf{x}} = M^{-1}\hat{\mathbf{x}}. \tag{4.4}$$

Without loss of generality, consider $\Gamma : \tilde{z} = a\tilde{x} + b\tilde{y} + c,\ (\tilde{x}, \tilde{y}) \in D$, where $a, b, c \in \mathbb{R}$ are constants, $D \subset \mathbb{R}^2$ is a bounded domain. By (4.4), we get $\hat{\Gamma} : \hat{z} = a(\frac{m_{\min}}{m_{\max}})\hat{x} + b(\frac{m_{\min}}{m_{\mathrm{mid}}})\hat{y} + cm_{\min},\ (\hat{x}, \hat{y}) \in \hat{D} \subset \mathbb{C}^2$, where $\hat{D}$ is a 2D bounded complex Euclidean domain. Obviously, $\frac{|D|}{|\hat{D}|} = |\det(\mathrm{diag}(m_{\max}^{-1}, m_{\mathrm{mid}}^{-1}))| = |m_{\max}|^{-1}|m_{\mathrm{mid}}|^{-1}$. Note that $m_{\max}$ and m_{mid} may be *complex*-valued.

Thus,

$$|\Gamma| = \iint_D \sqrt{1 + \tilde{z}_{\tilde{x}}^2 + \tilde{z}_{\tilde{y}}^2}\, \mathrm{d}\tilde{x}\, \mathrm{d}\tilde{y} = \sqrt{1 + a^2 + b^2}\ |D| \tag{4.5}$$

and

$$|\hat{\Gamma}| = \iint_{\hat{D}} \sqrt{1 + |\hat{z}_{\hat{x}}|^2 + |\hat{z}_{\hat{y}}|^2}\, \mathrm{d}\hat{x}\, \mathrm{d}\hat{y} = \sqrt{1 + a^2\left(\frac{|m_{\min}|}{|m_{\max}|}\right)^2 + b^2\left(\frac{|m_{\min}|}{|m_{\mathrm{mid}}|}\right)^2}\ |\hat{D}|. \tag{4.6}$$

Combining the above equalities, we get

$$\begin{aligned}\frac{|\Gamma|}{|\hat{\Gamma}|} &= |m_{\min}|^{-1}|m_{\mathrm{mid}}|^{-1}|m_{\max}|^{-1}\frac{\sqrt{1 + a^2 + b^2}}{\sqrt{\frac{1}{|m_{\min}|^2} + \frac{a^2}{|m_{\max}|^2} + \frac{b^2}{|m_{\mathrm{mid}}|^2}}} \\ &\le |m_{\min}|^{-1}|m_{\mathrm{mid}}|^{-1}|m_{\max}|^{-1}\frac{\sqrt{1 + a^2 + b^2}}{\sqrt{\frac{1}{|m_{\max}|^2} + \frac{a^2}{|m_{\max}|^2} + \frac{b^2}{|m_{\max}|^2}}} = |m_{\min}|^{-1}|m_{\mathrm{mid}}|^{-1}.\end{aligned} \tag{4.7}$$

□

4.2. Error analysis

Throughout this paper, we use C to denote a generic constant independent of A, ω, h, p, $\mathbf{E}$ and $\hat{\mathbf{E}}$.

We endow $\mathbf{V}(\mathcal{T}_h)$ with the mesh-skeleton norm,

$$\begin{aligned}|||\mathbf{w}|||_{\mathcal{F}_h}^2 &= \omega^{-1}\left\|\beta^{1/2}[\![\mu^{-1}\nabla_h \times \mathbf{w}]\!]_T\right\|_{0,\mathcal{F}_h^I}^2 + \omega\left\|\alpha^{1/2}[\![\mathbf{w}]\!]_T\right\|_{0,\mathcal{F}_h^I}^2 \\ &\quad + \omega^{-1}\left\|\delta^{1/2}\vartheta^{-1/2}\mathbf{n} \times \left(\mu^{-1}\nabla_h \times \mathbf{w}\right)\right\|_{0,\mathcal{F}_h^B}^2 + \omega\left\|(1-\delta)^{1/2}\vartheta^{1/2}\mathbf{n} \times \mathbf{w}\right\|_{0,\mathcal{F}_h^B}^2\end{aligned} \tag{4.8}$$

and the following augmented norm

$$\begin{aligned}|||\mathbf{w}|||_{\mathcal{F}_h^+}^2 &= |||\mathbf{w}|||_{\mathcal{F}_h}^2 + \omega\left\|\beta^{-1/2}\{\{\mathbf{w}\}\}\right\|_{0,\mathcal{F}_h^I}^2 \\ &\quad + \omega^{-1}\left\|\alpha^{-1/2}\{\{\mu^{-1}\nabla_h \times \mathbf{w}\}\}\right\|_{0,\mathcal{F}_h^I}^2 + \omega\left\|\delta^{-1/2}\vartheta^{1/2}(\mathbf{n} \times \mathbf{w})\right\|_{0,\mathcal{F}_h^B}^2.\end{aligned} \tag{4.9}$$

As in [8], we can show the following existence, uniqueness and continuity results of solution of the above variational problem.

Lemma 4.3. *There exists a unique solution* $\mathbf{E}_h$ *of* (2.8)*. Moreover, we have*

$$\begin{aligned}&-\mathrm{Im}[\mathcal{A}_h(\mathbf{w}, \mathbf{w})] = |||\mathbf{w}|||_{\mathcal{F}_h}^2, \\ &\text{and}\quad \left|\mathcal{A}_h(\mathbf{w}, \boldsymbol{\xi})\right| \le 2|||\mathbf{w}|||_{\mathcal{F}_h^+}\ |||\boldsymbol{\xi}|||_{\mathcal{F}_h},\quad \forall\ \mathbf{w}, \boldsymbol{\xi} \in \mathbf{V}(\mathcal{T}_h).\end{aligned} \tag{4.10}$$

The abstract error estimate built in [8] also holds in the current situation with the $\|\!|\cdot|\!\|_{\mathcal{F}_h}$-norm.

Lemma 4.4. *Let* $\mathbf{E}$ *be the analytical solution of* (2.1), (2.2) *and let* $\mathbf{E}_h$ *be the approximate solution of* (3.15). *Then, we have*

$$\|\!|\mathbf{E}-\mathbf{E}_h|\!\|_{\mathcal{F}_h} \leq 3 \inf_{\boldsymbol{\xi}_h\in\mathbf{V}_p(\mathcal{T}_h)} \|\!|\mathbf{E}-\boldsymbol{\xi}_h|\!\|_{\mathcal{F}_h^+}. \tag{4.11}$$

Completely different from the definition introduced in [8], we endow $\hat{\mathbf{V}}(\hat{\mathcal{T}}_{\hat{h}})$ with the mesh-skeleton norm

$$\|\!|\hat{\mathbf{w}}|\!\|^2_{\hat{\mathcal{F}}_{\hat{h}}} = \sum_k \left(\omega^{-1} \left\|\hat{\nabla}_{\hat{h}}\times\hat{\mathbf{w}}_k\right\|^2_{0,\partial\hat{\Omega}_k} + \omega \left\|\hat{\mathbf{w}}_k\right\|^2_{0,\partial\hat{\Omega}_k}\right). \tag{4.12}$$

The following intermediate result, which states the transformation stability with respect to two mesh-dependent norms, will play a key role in the derivation of the desired error estimates.

Lemma 4.5. *For* $\mathbf{E}\in\mathbf{V}(\mathcal{T}_h)$, *we have*

$$\|\!|\mathbf{E}|\!\|_{\mathcal{F}_h}, \|\!|\mathbf{E}|\!\|_{\mathcal{F}_h^+} \leq CC_2 \ \|\!|\hat{\mathbf{E}}|\!\|_{\hat{\mathcal{F}}_{\hat{h}}}, \tag{4.13}$$

where $C_2 = \max_k(|m^{(k)}_{\text{mid}}|^{-\frac{1}{2}} \ |m^{(k)}_{\min}|^{-\frac{1}{2}})\cdot(\max_k(\|\Lambda_k^{-\frac{1}{2}}\|)+\max_k(\rho_k^{\frac{1}{2}}))$.

Proof. We divide the proof into three steps.

Step 1. To estimate $\|[\![\mu^{-1}\nabla_h\times\mathbf{E}]\!]_T\|_{0,\mathcal{F}_h^I}$ and $\|\mathbf{n}\times(\mu^{-1}\nabla_h\times\mathbf{E})\|_{0,\mathcal{F}_h^B}$.

By the first equation of (3.3) and the first equation of (3.7), we can verify that

$$\mu_k^{-1}\nabla_h\times\mathbf{E}_k = \mu_{r,k}^{-1}\ P_k^T\Lambda_k^{-\frac{1}{2}}\ \hat{\nabla}_{\hat{h}}\times\hat{\mathbf{E}}_k. \tag{4.14}$$

Thus, we have, on the interface $\Gamma_{kj}\in\mathcal{F}_h^I$

$$[\![\mu^{-1}\nabla_h\times\mathbf{E}]\!]_T = \mathbf{n}_k\times\left(P_k^T\Lambda_k^{-\frac{1}{2}}\ \mu_{r,k}^{-1}\ \hat{\nabla}_{\hat{h}}\times\hat{\mathbf{E}}_k\right) + \mathbf{n}_j\times\left(P_j^T\Lambda_j^{-\frac{1}{2}}\ \mu_{r,j}^{-1}\ \hat{\nabla}_{\hat{h}}\times\hat{\mathbf{E}}_j\right). \tag{4.15}$$

It follows that, by the transformation (3.5)

$$\mathbf{n}_k = \left|S_k^{-T}\mathbf{n}_k\right|\ S_k^T\hat{\mathbf{n}}_k = \left|S_k^{-T}\mathbf{n}_k\right|\ P_k^T M_k^T\hat{\mathbf{n}}_k. \tag{4.16}$$

Notice that for $\forall\mathbf{a},\mathbf{b}\in\mathbb{C}^3, (P_k^T\mathbf{a})\times(P_k^T\mathbf{b}) = P_k^T(\mathbf{a}\times\mathbf{b})$. Then, by (4.16) we get

$$\begin{aligned}\mathbf{n}_k\times\left(P_k^T\Lambda_k^{-\frac{1}{2}}\ \nabla_{\hat{h}}\times\hat{\mathbf{E}}_k\right) &= \left|S_k^{-T}\mathbf{n}_k\right|\ \left(P_k^T M_k^T\hat{\mathbf{n}}_k\right)\times\left(P_k^T\Lambda_k^{-\frac{1}{2}}\ \hat{\nabla}_{\hat{h}}\times\hat{\mathbf{E}}_k\right)\\ &= \left|S_k^{-T}\mathbf{n}_k\right|\ P_k^T\left(\left(M_k^T\hat{\mathbf{n}}_k\right)\times\left(\Lambda_k^{-\frac{1}{2}}\ \hat{\nabla}_{\hat{h}}\times\hat{\mathbf{E}}_k\right)\right)\\ &= \left|S_k^{-T}\mathbf{n}_k\right|\ P_k^T\Lambda_k^{\frac{1}{2}}\hat{\mathbf{n}}_k\times\left(\hat{\nabla}_{\hat{h}}\times\hat{\mathbf{E}}_k\right).\end{aligned} \tag{4.17}$$

Substituting (4.17) into (4.15) yields

$$[\![\mu^{-1}\nabla_h\times\mathbf{E}]\!]_T = \left|S_k^{-T}\mathbf{n}_k\right|\ P_k^T\Lambda_k^{\frac{1}{2}}\hat{\mathbf{n}}_k\times\left(\mu_{r,k}^{-1}\ \hat{\nabla}_{\hat{h}}\times\hat{\mathbf{E}}_k\right) + \left|S_j^{-T}\mathbf{n}_j\right|\ P_j^T\Lambda_j^{\frac{1}{2}}\hat{\mathbf{n}}_j\times\left(\mu_{r,j}^{-1}\ \hat{\nabla}_{\hat{h}}\times\hat{\mathbf{E}}_j\right). \tag{4.18}$$

It is easy to see that

$$\left|S_k^{-T}\mathbf{n}_k\right|\ \left\|\Lambda_k^{-\frac{1}{2}}\right\| \leq \rho_k^{1/2}. \tag{4.19}$$

These, together with (4.18) and (4.3), lead to

$$\left\| [\![\mu^{-1}\nabla_h \times \mathbf{E}]\!]_T \right\|_{0,\mathcal{F}_h^I}^2 \le C\left(\max_k\left(\rho_k \left|m_{\text{mid}}^{(k)}\right|^{-1} \left|m_{\text{min}}^{(k)}\right|^{-1}\right)\right)\sum_k \left\|\hat{\nabla}_{\hat{h}} \times \hat{\mathbf{E}}_k\right\|_{0,\partial\hat{\Omega}_k}^2, \tag{4.20}$$

and

$$\left\|\mathbf{n} \times \left(\mu^{-1}\nabla_h \times \mathbf{E}\right)\right\|_{0,\mathcal{F}_h^B}^2 \le C\left(\max_k\left(\rho_k \left|m_{\text{mid}}^{(k)}\right|^{-1} \left|m_{\text{min}}^{(k)}\right|^{-1}\right)\right)\sum_k \left\|\hat{\nabla}_{\hat{h}} \times \hat{\mathbf{E}}_k\right\|_{0,\partial\hat{\Omega}_k}^2. \tag{4.21}$$

Step 2. Build estimates of $\|[\![\mathbf{E}]\!]_T\|_{0,\mathcal{F}_h^I}$ and $\|\mathbf{n}\times\mathbf{E}\|_{0,\mathcal{F}_h^B}$.

By the scaling transformation (3.2), the coordinate transformation (3.5) and (4.16), we have

$$\mathbf{n}_k \times \mathbf{E}_k = \left|S_k^{-T}\mathbf{n}_k\right| \left(P_k^T M_k^T \hat{\mathbf{n}}_k\right) \times \left(P_k^T \Lambda_k^{-\frac{1}{2}} \hat{\mathbf{E}}_k\right). \tag{4.22}$$

By direct manipulation, we can prove

$$\mathbf{n}_k \times \mathbf{E}_k = \left|S_k^{-T}\mathbf{n}_k\right| \; P_k^T \Lambda_k^{\frac{1}{2}} \; \hat{\mathbf{n}}_k \times \hat{\mathbf{E}}_k. \tag{4.23}$$

Combining (4.23) with (4.19) and (4.3) yields

$$\begin{aligned}
\|[\![\mathbf{E}]\!]_T\|_{0,\mathcal{F}_h^I}^2 &\le C\left(\max_k\left(\rho_k \left|m_{\text{mid}}^{(k)}\right|^{-1} \left|m_{\text{min}}^{(k)}\right|^{-1}\right)\right)\sum_k \left\|\hat{\mathbf{E}}_k\right\|_{0,\partial\hat{\Omega}_k}^2,\\
\|\mathbf{n}\times\mathbf{E}\|_{0,\mathcal{F}_h^B}^2 &\le C\left(\max_k\left(\rho_k \left|m_{\text{mid}}^{(k)}\right|^{-1} \left|m_{\text{min}}^{(k)}\right|^{-1}\right)\right)\sum_k \left\|\hat{\mathbf{E}}_k\right\|_{0,\partial\hat{\Omega}_k}^2.
\end{aligned} \tag{4.24}$$

Step 3. To estimate $\|\{\{\mathbf{E}\}\}\|_{0,\mathcal{F}_h^I}$, $\|\{\{\mu^{-1}\nabla_h\times\mathbf{E}\}\}\|_{0,\mathcal{F}_h^I}$ and $\|\mathbf{n}\times\mathbf{E}\|_{0,\mathcal{F}_h^B}$.

By the scaling transformation (3.2) and the coordinate transformation (3.5), we get

$$\|\{\{\mathbf{E}\}\}\|_{0,\mathcal{F}_h^I}^2 = \left\|\{\{G\tilde{\mathbf{E}}\}\}\right\|_{0,\mathcal{F}_h^I}^2 \le C\left(\max_k\left(\|\Lambda_k^{-1}\| \left(m_{\text{mid}}^{(k)}\right)^{-1} \left(m_{\text{min}}^{(k)}\right)^{-1}\right)\right)\sum_k \left\|\hat{\mathbf{E}}_k\right\|_{0,\partial\hat{\Omega}_k}^2. \tag{4.25}$$

Moreover, we have

$$\begin{aligned}
\left\|\left\{\left\{\mu^{-1}\nabla_h\times\mathbf{E}\right\}\right\}\right\|_{0,\mathcal{F}_h^I}^2 &\overset{(4.14)}{=\!=\!=} \left\|\left\{\left\{\mu_r^{-1}\; P^T\Lambda^{-\frac{1}{2}}\; \hat{\nabla}_{\hat{h}}\times\hat{\mathbf{E}}\right\}\right\}\right\|_{0,\mathcal{F}_h^I}^2\\
&\le C\left(\max_k\left(\|\Lambda_k^{-1}\| \left|m_{\text{mid}}^{(k)}\right|^{-1} \left|m_{\text{min}}^{(k)}\right|^{-1}\right)\right)\sum_k \left\|\hat{\nabla}_{\hat{h}}\times\hat{\mathbf{E}}_k\right\|_{0,\partial\hat{\Omega}_k}^2,
\end{aligned} \tag{4.26}$$

and

$$\|\mathbf{n}\times\mathbf{E}\|_{0,\mathcal{F}_h^B}^2 \overset{(4.24)}{\le} C\left(\max_k\left(\rho_k \left|m_{\text{mid}}^{(k)}\right|^{-1} \left|m_{\text{min}}^{(k)}\right|^{-1}\right)\right)\sum_k \left\|\hat{\mathbf{E}}_k\right\|_{0,\partial\hat{\Omega}_k}^2. \tag{4.27}$$

Combining (4.20), (4.21) with (4.24)–(4.27) gives the desired results (4.13).

□

For a bounded and connected domain $D\subset\Omega$, let $\|\cdot\|_{s,\omega,D}$ be the ω-weighted Sobolev norm defined by

$$\|\mathbf{E}\|_{s,\omega,D}^2 = \sum_{j=0}^{s}\omega^{2(s-j)}|\mathbf{E}|_{j,D}^2.$$

Set $\hat{\lambda} = \min_{\hat{\Omega}_k \in \hat{\mathcal{T}}_{\hat{h}}} \hat{\lambda}_k$, where $\hat{\lambda}_k$ is the positive parameter depending only on the shape of an element $\hat{\Omega}_k$ of $\hat{\mathcal{T}}_{\hat{h}}$ introduced in Theorem 3.2 of [19]. Let m satisfy $m \geq 2\ (1 + 2^{1/\hat{\lambda}})$.

The following approximation property is a direct consequence of Corollary 5.5 introduced in [8].

Lemma 4.6. *Assume that the analytical solution $\hat{\mathbf{E}} \in \mathbf{H}^{r+1}(curl; \hat{\Omega})$ satisfies the Maxwell equations (3.8) in isotropic media. Choose a set of p plane wave propagation directions $\{\mathbf{d}_l\}_{1 \leq l \leq p}$ with the corresponding set of polarization directions $\mathbf{F}_l, \mathbf{G}_l$ defined by (3.10) in a suitable manner. Assume that $1 < r \leq \frac{m-1}{2}$, and each element $\hat{\Omega}_k$ is star-shaped with respect to a ball. Then, there is a function $\hat{\boldsymbol{\xi}}_{\hat{h}} \in \hat{\mathbf{V}}_p(\hat{\mathcal{T}}_{\hat{h}})$ such that, for large p,*

$$\left|\!\left|\!\left|\hat{\mathbf{E}} - \hat{\boldsymbol{\xi}}_{\hat{h}}\right|\!\right|\!\right|_{\hat{\mathcal{F}}^+_{\hat{h}}} \leq C_3\ \omega^{-5/2} \left(\frac{\hat{h}}{m^{\hat{\lambda}}}\right)^{r-\frac{3}{2}} \left\|\hat{\nabla} \times \hat{\mathbf{E}}\right\|_{r+1,\omega,\hat{\Omega}}, \tag{4.28}$$

where $C_3 = C_3(\omega\hat{h}) > 0$ is independent of p and $\hat{\mathbf{E}}$, but increases as a function of the product $\omega\hat{h}$, and C_1 depends on the shape of the $\hat{\Omega}_k \in \hat{\mathcal{T}}_{\hat{h}}$, the index r, the material parameters $\vartheta, \varepsilon_r, \mu_r$ and the stabilization parameters.

With the help of the above preparation, we can prove the final results.

Theorem 4.7. *Let $\mathbf{E}$ and $\mathbf{E}_h$ denote the analytical solution of (2.1), (2.2) and the solution of (3.15), respectively. Suppose that p and r satisfy the conditions in Lemma 4.6. Then, for sufficiently large p, we have*

$$\left|\!\left|\!\left|\mathbf{E} - \mathbf{E}_h\right|\!\right|\!\right|_{\mathcal{F}_h} \leq C_3\ \tilde{C}\ \omega^{-5/2} \left(\frac{h}{m^{\hat{\lambda}}}\right)^{r-\frac{3}{2}} \|\nabla \times \mathbf{E}\|_{r+1,\omega,\Omega}, \tag{4.29}$$

where C_3 denotes the same positive number as in Lemma 4.6, the constant $\tilde{C}$ is defined as $\tilde{C} = C_1^{r-\frac{3}{2}} C_2 C_4 = (\max_k \|M_k\|)^{r-\frac{3}{2}} \max_k(|m_{\text{mid}}^{(k)}|^{-\frac{1}{2}}\ \ |m_{\min}^{(k)}|^{-\frac{1}{2}}) \cdot (\max_k(\|\Lambda_k^{-\frac{1}{2}}\|) + \max_k(\rho_k^{\frac{1}{2}})) \cdot (\max_k(|\det(M_k)|^{\frac{1}{2}}\ \|\Lambda_k^{-\frac{1}{2}}\|\ \|M_k^{-1}\|^{(r+1)}))$.

Proof. With the transformations (3.2) and (3.5), we define $\boldsymbol{\xi}_h(\mathbf{x}) = G\,\hat{\boldsymbol{\xi}}_{\hat{h}}(S\mathbf{x})$, where $\hat{\boldsymbol{\xi}}_{\hat{h}}$ satisfying (4.28) denotes the plane wave approximation of the scaled electric field $\hat{\mathbf{E}}$. Thus, by (4.11) and (4.13), together with (4.28) and (4.2), we deduce that

$$\begin{aligned}
\left|\!\left|\!\left|\mathbf{E} - \mathbf{E}_h\right|\!\right|\!\right|_{\mathcal{F}_h} &\overset{(4.11)}{\leq} C\ \left|\!\left|\!\left|\mathbf{E} - \boldsymbol{\xi}_h\right|\!\right|\!\right|_{\mathcal{F}^+_h} \overset{(4.13)}{\leq} C\ C_2 \left|\!\left|\!\left|\hat{\mathbf{E}} - \hat{\boldsymbol{\xi}}_{\hat{h}}\right|\!\right|\!\right|_{\hat{\mathcal{F}}^+_{\hat{h}}} \\
&\overset{(4.28)}{\leq} C\ C_2\ C_3 \omega^{-5/2} \left(\frac{\hat{h}}{m^{\hat{\lambda}}}\right)^{r-\frac{3}{2}} \left\|\hat{\nabla} \times \hat{\mathbf{E}}\right\|_{r+1,\omega,\hat{\Omega}} \\
&\overset{(4.2)}{\leq} C\ C_2\ C_3\ C_1^{r-\frac{3}{2}} \omega^{-5/2} \left(\frac{h}{m^{\hat{\lambda}}}\right)^{r-\frac{3}{2}} \left\|\hat{\nabla} \times \hat{\mathbf{E}}\right\|_{r+1,\omega,\hat{\Omega}}.
\end{aligned} \tag{4.30}$$

By the first equations of (3.3) and (3.7), respectively, we can deduct that

$$\left(\hat{\nabla} \times \hat{\mathbf{E}}\right)(\hat{\mathbf{x}}) = \Lambda^{-\frac{1}{2}} P\ (\nabla \times \mathbf{E})(\mathbf{x}). \tag{4.31}$$

Further, combining (4.31) with the scaling argument, we obtain

$$\left\|\hat{\nabla} \times \hat{\mathbf{E}}\right\|_{r+1,\omega,\hat{\Omega}} = \left(\sum_k \left\|\hat{\nabla} \times \hat{\mathbf{E}}\right\|^2_{r+1,\omega,\hat{\Omega}_k}\right)^{\frac{1}{2}} = \left(\sum_k \left\|\Lambda^{-\frac{1}{2}} P\ (\nabla \times \mathbf{E})\right\|^2_{r+1,\omega,\hat{\Omega}_k}\right)^{\frac{1}{2}}$$

TABLE 1. Errors of approximations with respect to ρ.

ρ in $\Lambda^{(1)}$		2^2	2^3	2^4	2^5	2^6
$h=\frac{1}{4}$	$p=64$	5.23e−5	6.25e−4	4.99e−3	1.89e−2	5.74e−2
	$p=81$	8.33e−6	6.12e−5	8.52e−4	6.19e−3	2.93e−2
$h=\frac{1}{6}$	$p=64$	2.85e−5	3.37e−4	2.67e−3	1.05e−2	3.15e−2
	$p=81$	3.75e−6	2.75e−5	3.74e−4	2.75e−3	1.36e−2
ρ in $\Lambda^{(2)}$		2^5	2^6	2^7	2^8	2^9
$h=\frac{1}{4}$	$p=64$	1.68e−3	4.73e−3	2.60e−2	1.64e−5	1.13e−3
	$p=81$	2.76e−4	2.05e−4	4.55e−4	1.13e−4	5.00e−5
$h=\frac{1}{6}$	$p=64$	9.17e−4	2.59e−3	1.42e−2	5.78e−4	8.19e−4
	$p=81$	1.28e−4	9.11e−5	2.12e−4	4.69e−5	1.27e−5

$$\leq \left(\sum_k |\det(M_k)| \left\|\Lambda_k^{-\frac{1}{2}}\right\|^2 \left\|M^{-1}\right\|^{2(r+1)} \|\nabla\times\mathbf{E}\|^2_{r+1,\omega,\Omega_k}\right)^{\frac{1}{2}}$$
$$\leq \left(\max_k\left(|\det(M_k)|^{\frac{1}{2}} \left\|\Lambda_k^{-\frac{1}{2}}\right\| \left\|M_k^{-1}\right\|^{(r+1)}\right)\right) \|\nabla\times\mathbf{E}\|_{r+1,\omega,\Omega}. \tag{4.32}$$

Denoting $C_4 = (\max_k(|\det(M_k)|^{\frac{1}{2}} \ \|\Lambda_k^{-\frac{1}{2}}\| \ \|M_k^{-1}\|^{(r+1)}))$, inserting (4.32) into (4.30), we get the desired result. □

Remark 4.8. For the case of homogeneous media, specially A is a constant matrix in the whole domain, then we have

$$\tilde{C} = |m_{\max}|^{\frac{1}{2}} \left\|\Lambda^{-\frac{1}{2}}\right\| \left(\left\|\Lambda^{-\frac{1}{2}}\right\| + \rho^{\frac{1}{2}}\right) \rho^{\frac{1}{2}\left(r-\frac{3}{2}\right)} \left\|M^{-1}\right\|^{\frac{5}{2}} \leq \rho^{\frac{1}{2}\left(r+\frac{1}{2}\right)} \left\|M^{-1}\right\|^{\frac{5}{2}} \left(1+\|A\|^{-\frac{1}{2}}\right). \tag{4.33}$$

5. LOCAL hp-REFINEMENT

For further improvement of accuracies of the approximations in the case of strong discontinuity media, we introduce a practically feasible local hp-refinement algorithm. Since it is hard to construct an analytic solution for the case of inhomogeneous media, we take the case of constant matrix A as an example. We consider the example tested in Section 6, but set the anisotropic matrix as $A = P^T\Lambda P$ in the whole domain Ω, where $P = \frac{1}{7}\begin{pmatrix} 6 & 2 & 3 \\ 3 & -6 & -2 \\ 2 & 3 & -6 \end{pmatrix}$. The exact solution of the problems satisfies (6.1).

5.1. An observation on generated isotropy media

We consider two different types of diagonal matrices: $\Lambda^{(1)} = \mathrm{diag}(-1, 1, \rho)$ and $\Lambda^{(2)} = \mathrm{diag}(-1, 1, \frac{1}{\rho})$, where ρ denotes the condition number of the anisotropic matrix A as usual. The L^2 relative errors of the approximations generated by the proposed PWDG method with respect to ρ are reported in Table 1 and Figure 1.

It can be seen from Table 1 that the accuracy of the approximation for the case of $\Lambda^{(2)}$ is significantly superior to that for the case of $\Lambda^{(1)}$. Besides, we can see from Figure 1 that the error performance of the resulting approximation $\mathbf{E}_h$ in terms of ρ for the case of local $\Lambda^{(2)}$ is superior to that for the case of $\Lambda^{(1)}$. Interestingly, it can be seen from Figure 1 (Right) that some errors will decline unexpectedly as the condition number increases.

The results listed in Table 1 and Figure 1 can be explained as follows: for the case of $\Lambda^{(1)}$ the coordinate transformation (3.5) maps the original domain Ω into larger regions $\hat{\Omega}$ (see Fig. 2 left) as the norm $\|S\|$ increases,

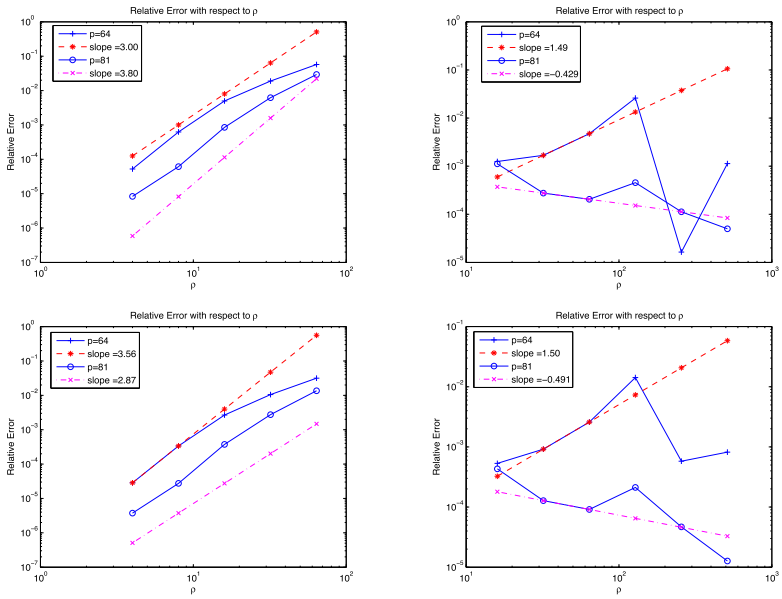

FIGURE 1. *Err. vs.* ρ in logarithmic scale. *Top row*: case of $h = \frac{1}{4}$; *Bottom row*: case of $h = \frac{1}{6}$. *Left*: case of $\Lambda^{(1)}$; *Right*: case of $\Lambda^{(2)}$.

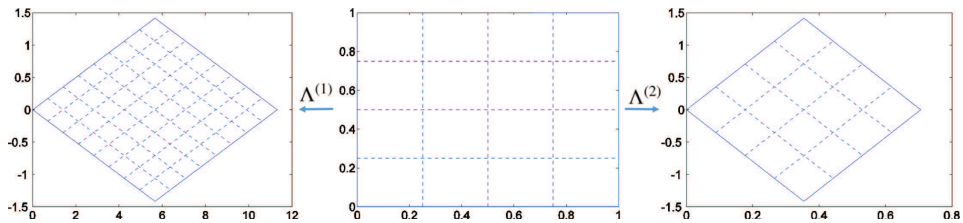

FIGURE 2. Transfer *anisotropy* to isotropy defined in the *sub-geometries* with different sizes for 2D case.

so larger number of plane wave basis functions is intrinsically required to approximate isotropic equations. On the contrary, for the case of $\Lambda^{(2)}$ the coordinate transformation (3.5) maps the original domain Ω into smaller regions $\hat{\Omega}$ (see Fig. 2 right) as the norm $\|S\|$ remains unchanging and ρ increases, so fewer plane wave basis functions is enough to approximate isotropic equations with higher accuracies.

Therefore, the essence of the scaling transformation and coordinate transformation is to transfer the *anisotropy* of the original equation to the isotropy defined in specially artificial *sub-geometries* with different sizes that do not intersect with each other, in which non physical electromagnetic field $(\hat{\mathbf{E}}(\hat{\mathbf{x}}), \hat{\mathbf{H}}(\hat{\mathbf{x}}))$ satisfies the element-by-element isotropic Maxwell equations.

5.2. A local *hp*-refinement algorithm

Notice that the coefficient matrices on different subdomains have different structure, so the *sub-geometries* after transformations have different sizes. According to the data in the last subsection, the accuracies of the approximate solutions of (3.15) depend on the structure for fixed discrete parameters h and p. This inspires us to introduce a practically feasible local *hp*-refinement algorithm to balance the structure so that the accuracies of the approximate solutions of (3.15) can be significantly improved.

Recall that Ω is divided into several subdomains $\{O_k\}$, and that ε_r, μ_r and the anisotropic matrix A are constant on each subdomain. Without loss of generality, we set $H_k = \mathrm{diam}(O_k) \approx 1$. Let $A_k = A|_{O_k}$ and $M_k = M|_{O_k}, S_k = S|_{O_k}$. Let $\hat{O}_k$ denote the image of O_k under the coordinate transformation (3.5), and let $\hat{H}_k$ be the diameter of $\hat{O}_k$. If the 2-norm sequence $\{\|S_k\|\}$ from the coordinate transformation (3.5) satisfies ascending order: $\|S_1\| \leq \|S_2\| \leq \|S_3\| \leq \cdots$, which indicates that $\hat{H}_1 \leq \hat{H}_2 \leq \hat{H}_3 \leq \cdots$. Then, we set $p_1 \leq p_2 \leq p_3 \leq \cdots$ in a proper way. That is, the number of basis functions p_k employed in subdomain O_k is adaptive to the diameter of the artificial sub-geometry $\hat{O}_k$ rather than that of the original subdomain O_k, namely, $p_k \propto \mathrm{diam}(\hat{O}_k)$.

For each O_k, let $\mathcal{T}_{h_k^s}$ and $\hat{\mathcal{T}}_{\hat{h}_k^s}$ respectively denote the triangulation of the subdomain O_k and the image of $\mathcal{T}_{h_k^s}$ under the coordinate transformation (3.5), where h_k^s and $\hat{h}_k^s$ denote the diameter of the maximal element in $\mathcal{T}_{h_k^s}$ and $\hat{\mathcal{T}}_{\hat{h}_k^s}$, respectively. We naturally have prior requirements $\hat{h}_1^s \approx \hat{h}_2^s \approx \hat{h}_3^s \approx \cdots \approx \hat{h}$. Then, according to the ascending order of the diameters of the artificial sub-geometries $\{\hat{O}_k\}$, the diameters of the triangulations $\mathcal{T}_{h_k^s}$ satisfy that $h_1^s \approx \mathcal{O}(\frac{\hat{h}}{\hat{H}_1}) \geq h_2^s \approx \mathcal{O}(\frac{\hat{h}}{\hat{H}_2}) \geq h_3^s \approx \mathcal{O}(\frac{\hat{h}}{\hat{H}_3}) \geq \cdots$. Of course, the triangulation $\mathcal{T}_h$ in the whole domain Ω is comprised of $\{\mathcal{T}_{h_k^s}\}$, which is conforming. Notice that, in the actual implementation of the proposed method, we need not calculate the virtual grids $\hat{\mathcal{T}}_{\hat{h}}$.

The practically feasible *hp*-refinement algorithm can be described as follows.

Algorithm 1. Local *hp*-refinement.

Compute the 2-norm $\{\|S_k\|\}$ of each subdomain O_k.
p-refinement: set p_k proportionally to $\|S_k\|$.
h-refinement: set the diameter h_k^s of the triangulation $\mathcal{T}_{h_k^s}$ proportionally to $\frac{\hat{h}}{\|S_k\|}$.

5.3. Error estimates

As stated above, we require that the virtual mesh $\hat{\mathcal{T}}_{\hat{h}}$ satisfies shape regular assumption. Then we can obtain a geometric property for the current triangulations.

Lemma 5.1. *For the proposed triangulation, we have*

$$\hat{h} \leq C \left(\max_k \left\| M_k^{-1} \right\|^{-1} \right) h. \tag{5.1}$$

Proof. By the assumption that the virtual mesh $\hat{\mathcal{T}}_{\hat{h}}$ satisfies shape regularity, we have on each subdomain O_k by Lemma 2.2 and (3.23) from [24],

$$\hat{h}_k^s \leq C \left\| M_k^{-1} \right\|^{-1} h_k^s. \tag{5.2}$$

By taking the maximum value, we can get the desired result. □

Similarly to the proof of Theorem 4.7, we can get the optimized error estimates with respect to the condition number of the piecewise constant anisotropic matrices.

Theorem 5.2. *Let $\mathbf{E} \in \mathbf{H}^{r+1}(curl;\Omega)$ and $\mathbf{E}_h$ denote the analytical solution of (2.1), (2.2) and the solution of (3.15), respectively. Choose $p_k = (m_k^O + 1)^2$ on each element of the subdomain O_k. Assume that $1 < r \leq \frac{m_k^O - 1}{2}$ for every k. Then, for sufficiently large p_k, we have*

$$\left\| \mathbf{E} - \mathbf{E}_h \right\|_{\mathcal{F}_h} \leq C_3 \, \tilde{C} \, \omega^{-5/2} \left(\frac{h}{m^{\hat{\lambda}}} \right)^{r - \frac{3}{2}} \|\nabla \times \mathbf{E}\|_{r+1,\omega,\Omega}, \tag{5.3}$$

where C_3 denotes the same positive number as in Lemma 4.6, $C_5 = (\max_k \|M_k^{-1}\|^{-1})$, the constant $\tilde{C}$ is defined as $\tilde{C} = C_5^{r-\frac{3}{2}} C_2 C_4 = (\max_k \|M_k^{-1}\|^{-1})^{r-\frac{3}{2}} \max_k(|m_{\text{mid}}^{(k)}|^{-\frac{1}{2}} \ |m_{\text{min}}^{(k)}|^{-\frac{1}{2}}) \cdot (\max_k(\|\Lambda_k^{-\frac{1}{2}}\|) + \max_k(\rho_k^{\frac{1}{2}})) \cdot (\max_k(|\det(M_k)|^{\frac{1}{2}} \ \|\Lambda_k^{-\frac{1}{2}}\| \ \|M_k^{-1}\|^{(r+1)}))$ and $m = \min_k m_k^O$.

Proof. The result follows from (4.30) and (4.32), with the particular usage of (5.1) and the number of basis functions p_k on each element of the subdomain O_k. □

Remark 5.3. For the case of homogeneous media, specially A is a constant matrix in the whole domain, then we have

$$\tilde{C} = |m_{\max}|^{\frac{1}{2}} \ \left\|\Lambda^{-\frac{1}{2}}\right\| \ \left(\left\|\Lambda^{-\frac{1}{2}}\right\| + \rho^{\frac{1}{2}}\right) \ \left\|M^{-1}\right\|^{\frac{5}{2}} \leq \rho \ \left(1 + \|A\|^{-\frac{1}{2}}\right) \ \left\|M^{-1}\right\|^{\frac{5}{2}}. \tag{5.4}$$

Compared with (4.33) on the assumption that $\mathcal{T}_h$ is shape regular, we obtain obviously better error estimates in the sense that the error bounds on the condition number ρ.

Remark 5.4. Although both the triangulations used in the literature [24] and this paper require that the mesh partitioning on non physical region $\hat{\Omega}$ meets the shape regular assumption, their implementation forms are completely different. For the case of homogeneous anisotropic media with the positive definite matrix, $\hat{\Omega}$ is decomposed into polyhedron elements $\{\hat{\Omega}_k\}$ such that $\hat{\mathcal{T}}_{\hat{h}}$ is shape regular. While for the current situation, we address that, the broader model studied here makes the transformed domain $\hat{\Omega}$ a complex-valued region, and partitioning it directly is expensive. Fortunately, the local *hp*-refinement algorithm can accomplish this assumption by partitioning the original domain Ω to generate the realistic mesh $\mathcal{T}_h$, so the mesh partitioning of the transformed domain $\hat{\Omega}$ at this time is a virtual mesh.

6. Numerical experiments

In this section, we apply the proposed PWDG method to solve the electromagnetic wave propagation in anisotropic media with piecewise constant symmetric matrices, and we report some numerical results to verify the efficiency of the proposed method.

We consider the choice of numerical fluxes for the PWDG method as in [24]: the constant parameters $\alpha = \beta = \delta = 1/2$, which is explained in Remark 2.1. To measure the accuracy of the numerical solutions $\mathbf{E}_h$, we introduce the following L^2 relative error:

$$\text{err.} = \frac{\|\mathbf{E} - \mathbf{E}_h\|_{\mathbf{L}^2(\Omega)}}{\|\mathbf{E}\|_{\mathbf{L}^2(\Omega)}}$$

for the exact solution $\mathbf{E} \in \mathbf{L}^2(\Omega)$. All of the computations have been done in MATLAB, and the discrete system was computed by the numerical integration on the mesh skeleton. The mesh $\mathcal{T}_h$ of Ω is generated by the software Gmsh [7].

We compute the electric field due to an electric dipole source at the point $\mathbf{x}_0 = (-0.6, -0.6, -0.6)$. The boundary data $\mathbf{g}$ can be computed by the referred solution $\mathbf{E}_{\text{ref}}$ satisfying a homogeneous Maxwell system (2.1):

$$\mathbf{E}_{\text{ref}} = -\mathrm{i}\omega\phi(\mathbf{x}, \mathbf{x}_0) G \ \mathbf{a} + \frac{1}{i\omega\varepsilon_r} G \ \nabla_{\hat{h}}(\nabla_{\hat{h}}\phi \cdot \mathbf{a}), \tag{6.1}$$

where

$$\phi(\mathbf{x}, \mathbf{x}_0) = \frac{\exp\left(\mathrm{i}\omega\sqrt{\varepsilon_r}|S \ \mathbf{x} - \mathbf{x}_0|\right)}{4\pi|S \ \mathbf{x} - \mathbf{x}_0|}$$

and $\Omega = [0, 1]^3$. Set $\varepsilon_r = \mu_r = 1$ and $\mathbf{a} = (\frac{1}{\sqrt{3}}, \frac{1}{\sqrt{3}}, \frac{1}{\sqrt{3}})^T$.

TABLE 2. Parameters of tetrahedral mesh.

Subdomain	Ω_1	Ω_2
Number of tetrahedrons	12 815	21 842

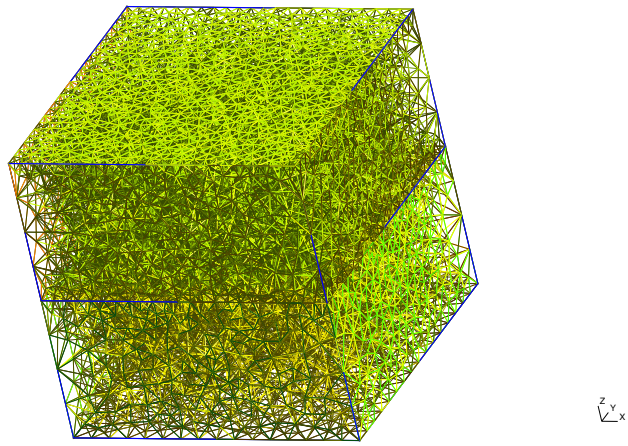

FIGURE 3. Tetrahedral mesh $\mathcal{T}_h$.

6.1. The case of two sub-geometries

Consider the case of inhomogeneous media:

$$\Lambda = \begin{cases} \Lambda_1 = \mathrm{diag}(-1, 1, \rho), & \Omega_1 : z < 0.5, \\ \Lambda_2 = \mathrm{diag}(1, -1, 2\rho), & \Omega_2 : z > 0.5. \end{cases} \tag{6.2}$$

The above two subdomains correspond to the orthogonal matrix: $P_1 = \frac{1}{7}\begin{pmatrix} 6 & 2 & 3 \\ 3 & -6 & -2 \\ 2 & 3 & -6 \end{pmatrix}$ on subdomain Ω_1, $P_2 = \begin{pmatrix} \frac{1}{\sqrt{2}} & 0 & -\frac{1}{\sqrt{2}} \\ 0 & 1 & 0 \\ \frac{1}{\sqrt{2}} & 0 & \frac{1}{\sqrt{2}} \end{pmatrix}$ on subdomain Ω_2.

We adopt a nonuniform tetrahedral mesh $\mathcal{T}_h$ for the domain Ω generated by the proposed Algorithm 1, which is shown in Table 2 and Figure 3 for the case of $\rho = 4$. In particular, as given in Algorithm 1, we set $h_1^s = \frac{1}{16}$ close to the plane $z = 0$, and $h_2^s = \frac{1}{23}$ close to the plane $z = 0.5$ or $z = 0.1$, which guarantees that $\frac{h_1^s}{h_2^s} \approx \frac{\|S_2\|}{\|S_1\|}$.

Figure 4 shows the z component of the approximate solutions for the free-space dipole at $\omega = 2\pi$. For the case of uniform hp finite element, we choose $h = \frac{1}{16}$ and the number p of basis functions as $p = 64$. For the case of feasible local hp-refinement technology, we choose the number p as $p = 64$ when $z > 0.5$, and $p = 49$ when $z < 0.5$.

Figure 4 shows that the local hp-refinement technology can generate much better approximations than the case of the uniform hp finite element.

It is hard to construct an analytic solution for the case in layered media. We consider the actual measurements of the solution error by taking the numerical solution on the above mesh and on the largest number of basis functions per element as a reference solution.

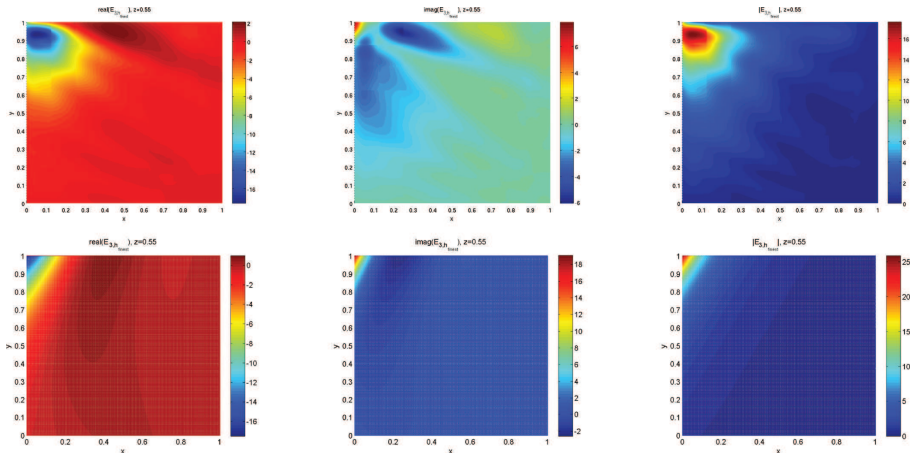

FIGURE 4. Numerical solutions. *Top row*: case of uniform *hp*; *Bottom row*: case of feasible local *hp*-refinement technology.

TABLE 3. Errors of approximations with respect to ρ.

ρ	2^2	2^3	2^4	2^5	2^6
Uniform *hp*	1.24e−3	2.02e−3	7.51e−3	2.27e−2	1.11e−1
Local *hp*	9.56e−4	1.32e−3	2.46e−3	4.57e−3	8.58e−3

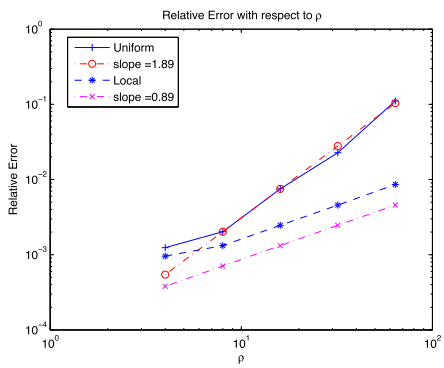

FIGURE 5. *Err. vs.* ρ in logarithmic scale.

The L^2 relative errors of the approximations generated by the proposed PWDG method with respect to ρ are reported in Table 3 and Figure 5. We fix $\omega = 2\pi$, but increase the condition number of the anisotropic matrix A. For the case of uniform *hp*, we choose the number p of basis functions as $p = 36$. For the case of feasible local *hp*-refinement technology, we choose the number p as $p = 25$ when $\mathbf{x} \in \Omega_1$, $p = 36$ when $\mathbf{x} \in \Omega_2$.

We can see from Figure 5 that, the local *hp*-refinement technology can generate much better approximations than the case of the uniform *hp* finite element, and the error performance of the resulting approximation $\mathbf{E}_h$ in terms of ρ for the case of local *hp*-refinement is superior to that for the case of the uniform *hp* finite element.

TABLE 4. Parameters of tetrahedral mesh.

Subdomain	Ω_1	Ω_2	Ω_3	Ω_4
Number of tetrahedrons	24 240	14 684	105 351	31 572

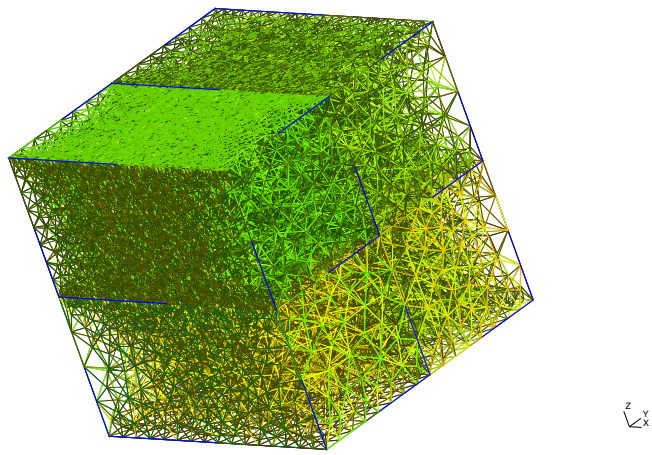

FIGURE 6. Tetrahedral mesh $\mathcal{T}_h$.

6.2. The case of four sub-geometries

Consider the case of inhomogeneous media:

$$\Lambda = \begin{cases} \Lambda_1 = \mathrm{diag}(-1, 1, \rho), & \Omega_1 := y < 0.5, z < 0.5, \\ \Lambda_2 = \mathrm{diag}(-1, 2, -\rho), & \Omega_2 := y > 0.5, z < 0.5, \\ \Lambda_3 = \mathrm{diag}(-\rho, 1, \rho), & \Omega_3 := y < 0.5, z > 0.5, \\ \Lambda_4 = \mathrm{diag}(2, 1, \rho), & \Omega_4 := y > 0.5, z > 0.5. \end{cases} \tag{6.3}$$

The above four subdomains correspond to the orthogonal matrix: $P_1 = \frac{1}{7}\begin{pmatrix} 6 & 2 & 3 \\ 3 & -6 & -2 \\ 2 & 3 & -6 \end{pmatrix}$ on subdomain Ω_1, $P_2 = \begin{pmatrix} \frac{1}{\sqrt{2}} & 0 & -\frac{1}{\sqrt{2}} \\ 0 & 1 & 0 \\ \frac{1}{\sqrt{2}} & 0 & \frac{1}{\sqrt{2}} \end{pmatrix}$ on Ω_2, $P_3 = \begin{pmatrix} -0.0842 & 0.7301 & -0.6782 \\ 0.5018 & 0.6191 & 0.6041 \\ 0.8609 & -0.2894 & -0.4185 \end{pmatrix}$ on Ω_3, and $P_4 = \begin{pmatrix} -1/\sqrt{3} & -1/\sqrt{3} & 1/\sqrt{3} \\ -1/\sqrt{2} & 1/\sqrt{2} & 0 \\ 1/\sqrt{6} & 1/\sqrt{6} & \sqrt{6}/3 \end{pmatrix}$ on Ω_4, respectively.

We adopt a nonuniform tetrahedral mesh $\mathcal{T}_h$ for the domain Ω generated by the proposed Algorithm 1, which is shown in Table 4 and Figure 6.

Figure 7 shows the z component of the approximate solutions as a reference solution for the free-space dipole at $\omega = 2\pi$. For the case of uniform hp, we choose $h = \frac{1}{24}$ and the number p of basis functions as $p = 64$. For the case of feasible local hp-refinement technology, we choose the number p as $p = 49$ when $\mathbf{x} \in \Omega_1$, $p = 64$ when $\mathbf{x} \in \Omega_2$, $p = 81$ when $\mathbf{x} \in \Omega_3$, $p = 64$ when $\mathbf{x} \in \Omega_4$.

The L^2 relative errors of the approximations generated by the proposed PWDG method with respect to ρ are reported in Table 5 and Figure 8. We fix $\omega = 2\pi$, but increase the condition number of the anisotropic matrix

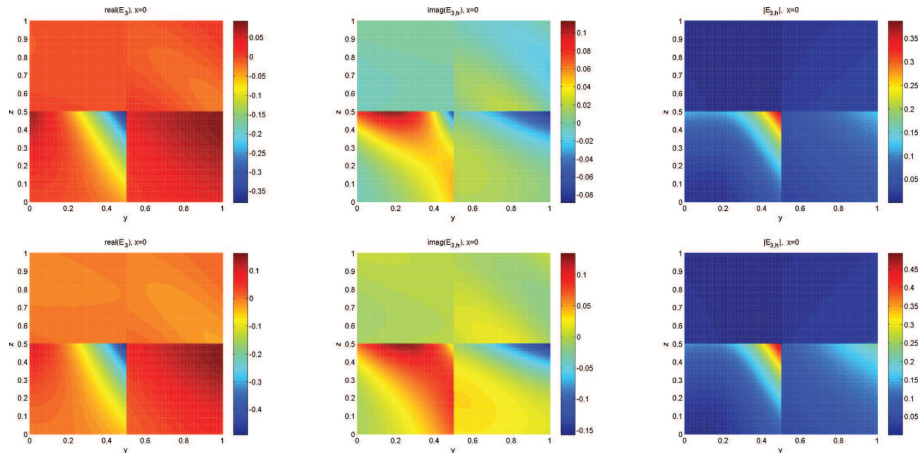

FIGURE 7. Numerical solutions. *Top row*: case of uniform *hp*; *Bottom row*: case of feasible local *hp*-refinement technology.

TABLE 5. Errors of approximations with respect to ρ.

ρ	2^2	2^3	2^4	2^5	2^6
Uniform *hp*	3.48e−4	1.19e−3	5.46e−3	2.12e−2	8.39e−2
Local *hp*	8.31e−5	3.02e−4	5.57e−4	1.14e−3	2.25e−3

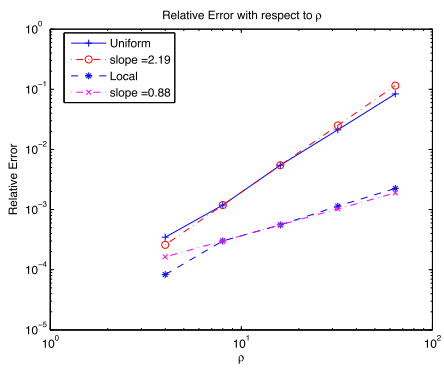

FIGURE 8. *Err. vs.* ρ in logarithmic scale.

A. For the case of uniform *hp*, we choose the number p of basis functions as $p = 36$. For the case of feasible local *hp*-refinement technology, we choose the number p as $p = 25$ when $\mathbf{x} \in \Omega_1$, $p = 36$ when $\mathbf{x} \in \Omega_2$, $p = 49$ when $\mathbf{x} \in \Omega_3$, $p = 36$ when $\mathbf{x} \in \Omega_4$.

We can see from Figure 8 that the local *hp*-refinement technology can generate much better approximations than the case of the uniform *hp* finite element. Besides, the error performance of the resulting approximation $\mathbf{E}_h$ in terms of ρ for the case of local *hp*-refinement is superior to that for the case of the uniform *hp* finite element.

7. Conclusion

In this paper we have introduced a plane wave discontinuous Galerkin method for discretization of the three-dimensional anisotropic time-harmonic inhomogeneous Maxwell equations with piecewise constant symmetric matrices, and derived the error estimate with respect to the condition number of the coefficient matrix of the resulting approximate solutions. Two different types of piecewise scaling transformations and coordinate transformations were proposed to define piecewise plane wave basis functions. We introduced the feasible local *hp*-refinement algorithm to substantially improve the resulting approximate accuracy.

Acknowledgements. The authors are very grateful to the anonymous referees for the careful reading of a preliminary version of the manuscript and their valuable suggestions and comments, which greatly improved the quality of this paper.

Funding. L. Yuan was supported by Shandong Provincial Natural Science Foundation under the grant ZR2020MA046 and Cultivation Project of Young and Innovative Talents in Universities of Shandong Province. Q. Hu was supported by the Natural Science Foundation of China G12071469.

References

[1] H. Ammari, B. Li and J. Zou, Mathematical analysis of electromagnetic scattering by dielectric nanoparticles with high refractive indices. *Trans. Am. Math. Soc.* **376** (2023) 39–90.

[2] G. Bao, H. Zhang and J. Zou, Unique determination of periodic polyhedral structures by scattered electromagnetic fields. *Trans. Am. Math. Soc.* **363** (2011) 4527–4551.

[3] A. Buffa, Remarks on the discretization of some noncoercive operator with applications to heterogeneous Maxwell equations. *SIAM J. Numer. Anal.* **43** (2005) 1–18.

[4] A. Buffa and R. Hiptmair, A coercive combined field integral equation for electromagnetic scattering. *SIAM J. Numer. Anal.* **42** (2004) 621–640.

[5] O. Cessenat, *Application d'une nouvelle formulation variationnelle aux équations d'ondes harmoniques, Problèmes de Helmholtz 2D et de Maxwell 3D.* Ph.D. Thesis, Université Paris IX Dauphine (1996).

[6] W. Chew, Waves and Fields in Inhomogeneous Media. IEEE, New York (1995).

[7] C. Geuzaine and J. Remacle, GMSH: a three-dimensional finite element mesh generator with built-in pre- and post-processing facilities. *Int. J. Numer. Meth. Eng.* **79** (2009) 1309–1331.

[8] R. Hiptmair, A. Moiola and I. Perugia, Error analysis of Trefftz-discontinuous Galerkin methods for the time-harmonic Maxwell equations. *Math. Comput.* **82** (2013) 247–268.

[9] Q. Hu and R. Song, A variant of the plane wave least squares method for the time-harmonic Maxwell's equations. *ESAIM: M2AN Math. Model. Numer. Anal.* **53** (2019) 85–103.

[10] Q. Hu and L. Yuan, A plane wave least-squares method for time-harmonic Maxwell's equations in absorbing media. *SIAM J. Sci. Comput.* **36** (2014) A1911–A1936.

[11] Q. Hu and L. Yuan, A plane wave method combined with local spectral elements for nonhomogeneous Helmholtz equation and time-harmonic Maxwell equations. *Adv. Comput. Math.* **44** (2018) 245–275.

[12] Q. Hu and H. Zhang, Substructuring preconditioners for the systems arising from plane wave discretization of Helmholtz equations. *SIAM J. Sci. Comput.* **38** (2016) A2232–A2261.

[13] L. Imbert-Gerard, F. Vico, L. Greengard and M. Ferrando, Integral equation methods for electrostatics, acoustics, and electromagnetics in smoothly varying anisotropic media. *SIAM J. Numer. Anal.* **57** (2019) 1020–1035.

[14] J. Jackson, Classical Electrodynamics. Wiley, New York (1975).

[15] X. Jiang, W. Chen and C. Chen, Fast multipole accelerated boundary knot method for inhomogeneous Helmholtz problems. *Eng. Anal. Bound. Elem.* **37** (2013) 1239–1243.

[16] L. Landau, E. Lifshitz and L. Pitaevskii, Electrodynamics of Continuous Media. Pergamon Press, Oxford (1984).

[17] Q. Lu, J. Wang, S. Shu and J. Peng, Two-level overlapping Schwarz methods based on local generalized eigenproblems for Hermitian variational problems. *SIAM J. Sci. Comput.* **44** (2022) A605–A635.

[18] R. Marqués, F. Medina and R. Rafii-El-Idrissi, Role of bianisotropy in negative permeability and left-handed metamaterials. *Phys. Rev. B* **65** (2002) 144440.

[19] A. Moiola, R. Hiptmair and I. Perugia, Plane wave approximation of homogeneous Helmholtz solutions. *Z. Angew. Math. Phys.* **62** (2011) 809–837.

[20] Z. Sacks, D. Kingsland, R. Lee and J. Lee, A perfectly matched anisotropic absorber for use an absorbing boundary condition. *IEEE Trans. Antennas Propag.* **43** (1995) 1460–1463.

[21] N. Sloan, Tables of spherical codes (with collaboration of R.H. Hardin, W.D. Smith and others) published electronically at http://www2.research.att.com/njas/packings (2000).

[22] L. Yuan, A combined scheme of the local spectral element method and the generalized plane wave discontinuous Galerkin method for the anisotropic Helmholtz equation. *Appl. Numer. Math.* **150** (2020) 341–360.

[23] L. Yuan and Q. Hu, Error analysis of the plane wave discontinuous Galerkin method for Maxwell's equations in anisotropic media. *Commun. Comput. Phys.* **25** (2019) 1496–1522.

[24] L. Yuan and Q. Hu, Plane wave discontinuous Galerkin methods for the Helmholtz equation and Maxwell equations in anisotropic media. *Comput. Math. Appl.* **97** (2021) 355–374.

[25] L. Yuan and Q. Hu, A discontinuous plane wave neural network method for Helmholtz equation and time-harmonic Maxwell's equations. Submitted arXiv:2310.09527 (2023).

[26] M. Zhao, N. Zhu and L. Wang, The electromagnetic scattering from multiple arbitrarily shaped cavities with inhomogeneous anisotropic media. *J. Comput. Phys.* **489** (2023) 112274.